Atmos. Chem. Phys. Discuss., 13, 1795–1853, 2013
www.atmos-chem-phys-discuss.net/13/1795/2013/
doi:10.5194/acpd-13-1795-2013

Atmospheric Chemistry and Physics Discussions

Ozone photochemistry in boreal biomass burning plumes

M. Parrington[1], P. I. Palmer[1], A. C. Lewis[2], J. D. Lee[2], A. R. Rickard[3,*], P. Di Carlo[4,5], J. W. Taylor[6], J. R. Hopkins[2], S. Punjabi[7], D. E. Oram[8], G. Forster[8], E. Aruffo[4,5], S. J. Moller[2], S. J.-B. Bauguitte[9], J. D. Allan[6,10], H. Coe[6], and R. J. Leigh[11]

[1]School of GeoSciences, The University of Edinburgh, Edinburgh, UK
[2]National Centre for Atmospheric Science, Department of Chemistry, University of York, York, UK
[3]National Centre for Atmospheric Science, School of Chemistry, University of Leeds, UK
[4]Center of Excellence CETEMPS, University of L'Aquila, L'Aquila, Italy
[5]Department of Physical and Chemical Sciences, University of L'Aquila, L'Aquila, Italy
[6]School of Earth, Atmospheric and Environmental Sciences, University of Manchester, Manchester, UK
[7]Department of Chemistry, University of York, York, UK
[8]National Centre for Atmospheric Science, School of Environmental Sciences, University of East Anglia, Norwich, UK
[9]Facility for Airborne Atmospheric Measurements, Bedford, UK
[10]National Centre for Atmospheric Science, University of Manchester, Manchester, UK

[11]Department of Physics and Astronomy, University of Leicester, Leicester, UK
[*]now at: the National Centre for Atmospheric Science, Department of Chemistry, University of York, York, UK

Received: 26 December 2012 – Accepted: 8 January 2013 – Published: 17 January 2013

Correspondence to: M. Parrington (mark.parrington@ed.ac.uk)

Published by Copernicus Publications on behalf of the European Geosciences Union.

Abstract

We present an analysis of ozone photochemistry observed by aircraft measurements of boreal biomass burning plumes over Eastern Canada in the summer of 2011. Measurements of ozone and a number of key chemical species associated with ozone photochemistry, including non-methane hydrocarbons (NMHCs), nitrogen oxides (NO_x) and total nitrogen containing species (NO_y), were made from the UK FAAM BAe-146 research aircraft as part of the quantifying the impact of BOReal forest fires on tropospheric oxidants over the Atlantic using Aircraft and Satellites (BORTAS) experiment between 12 July and 3 August 2011. We found that ozone mixing ratios measured in biomass burning plumes were indistinguishable from non-plume measurements, but evaluating them in relationship to measurements of carbon monoxide (CO), total alkyl nitrates (ΣAN) and the surrogate species NO_z ($= NO_y - NO_x$) revealed that the potential for ozone production increased with plume age. We used NMHC ratios to estimate photochemical ages of the observed biomass burning plumes between 0 and 15 days. Ozone production, calculated from $\Delta O_3/\Delta CO$ enhancement ratios, increased from $0.020 \pm 0.008\,\mathrm{ppbv\,ppbv^{-1}}$ in plumes with photochemical ages less than 2 days to $0.55 \pm 0.29\,\mathrm{ppbv\,ppbv^{-1}}$ in plumes with photochemical ages greater than 5 days. In comparing ozone mixing ratios with components of the NO_y budget we observed that plumes with ages between 2 and 4 days were characterised by high aerosol loading, relative humidity greater than 40 %, and low ozone production efficiencies of $8\,\mathrm{ppbv\,ppbv^{-1}}$ relative to ΣAN and $2\,\mathrm{ppbv\,ppbv^{-1}}$ relative to NO_z. In plumes with ages greater than 4 days, ozone production efficiency increased to $473\,\mathrm{ppbv\,ppbv^{-1}}$ relative to ΣAN and $155\,\mathrm{ppbv\,ppbv^{-1}}$ relative to NO_z. From the BORTAS measurements we estimated that aged plumes with low aerosol loading were close to being in photostationary steady state and ozone production in younger plumes was inhibited by high aerosol loading and greater production of ΣAN relative to ozone. The BORTAS measurements of ozone photochemistry in boreal biomass burning plumes were found to be consistent with previous summertime aircraft measurements made over the same

Title Page
Abstract | Introduction
Conclusions | References
Tables | Figures
◀| |▶
◀ ▶
Back | Close
Full Screen / Esc
Printer-friendly Version
Interactive Discussion

region during the Arctic Research of the Composition of the troposphere (ARCTAS-B) in 2008 and Atmospheric Boundary Layer Experiment (ABLE 3B) in 1990.

1 Introduction

The quantifying the impact of BOReal forest fires on tropospheric oxidants over the Atlantic using Aircraft and Satellites (BORTAS) experiment was conducted in two phases during July–August 2010 (phase A) and 2011 (phase B) (Palmer et al., 2012). The overarching objective of BORTAS was to better understand the chemical evolution of plumes emitted from wildfires in boreal regions, with a particular emphasis on the net production tropospheric ozone, and downwind impacts on air quality. The first phase of the experiment (BORTAS-A) comprised of ground-based, ozonesonde, and satellite measurements over Eastern Canada in the summer of 2010, the results of which were reported by Parrington et al. (2012). The second phase of the experiment (BORTAS-B) was an aircraft measurement campaign based out of Halifax, Nova Scotia, Canada between 12 July and 3 August 2011, supported by ground-based, ozonesonde, and satellite measurements. An overview of the BORTAS-B campaign is given by Palmer et al. (2012). In this paper we analyse ozone photochemistry in the biomass burning plumes sampled by the aircraft during BORTAS-B.

Ozone in the troposphere is a secondary pollutant formed by the photo-oxidation of carbon monoxide (CO) and volatile organic compounds (VOCs) in the presence of nitrogen oxides (NO_x) and transport from the stratosphere. Removal of ozone from the troposphere is through dry deposition and photochemical destruction. Tropospheric ozone plays an important role in the contexts of climate and air quality through its influence on tropospheric chemistry as a precursor of the hydroxyl radical (OH) which is the principal atmospheric oxidant, with the photochemistry controlling its production also implicated in photochemical smog formation. Emissions of the ozone precursors (i.e. NO_x and VOCs) can be anthropogenic in origin and can also have natural sources such as biogenic processes and biomass burning. A number of previous measurement campaigns have made in situ observations of photochemistry within boreal biomass burning outflow and evaluated the associated ozone production and loss. The NASA Atmospheric Boundary Layer Experiment (ABLE) included two high-latitude aircraft measurement campaigns in the summers of 1988 (ABLE 3A) and 1990 (ABLE 3B) (Harriss et al., 1992, 1994). Analysis of the ABLE 3A measurements, made over northern and western Alaska, found ozone production in haze layers associated with fires to be inefficient with less than 0.1 molecules of ozone formed per molecule of CO (Wofsy et al., 1992). The ABLE 3B measurements, made over Central and Eastern Canada, did observe ozone enhancements of 5–15 ppbv in aged (> 2 days) biomass burning plumes (Anderson et al., 1994). Aircraft measurements made over the North Atlantic Ocean during the Intercontinental Transport of Ozone and Precursors (ITOP) campaign (Lewis et al., 2007), which was part of the wider International Consortium for Atmospheric Research on Transport and Transformation (ICARTT) (Fehsenfeld et al., 2006) in the summer of 2004, sampled biomass burning plumes associated with fires in Alaska. Examples of elevated ozone were observed in individual plumes with elevated CO during ITOP but there was no single canonical relationship (Lewis et al., 2007). More recently the NASA Arctic Research of the Composition of the troposphere from Aircraft and Satellites (ARCTAS) campaign in the spring and summer of 2008 made measurements of biomass burning plumes in Central Canada. Analysis of the ARCTAS aircraft measurements showed little evidence for ozone formation within the plumes (Alvarado et al., 2010) other than when the plumes were mixed with outflow from urban pollution (Singh et al., 2010). Ground-based measurements of outflow from boreal biomass burning have also been routinely made at the Pico Mountain Observatory in the mid-Atlantic (Lapina et al., 2006; Val Martin et al., 2006; Helmig et al., 2008). Years with high boreal fire activity have been shown to increase ozone mixing ratios in the free troposphere over this site by up to 10 ppbv (Lapina et al., 2006) with photochemically aged biomass burning plumes influencing tropospheric oxidant chemistry after 1–2 weeks of transport to the region (Helmig et al., 2008).

Model analyses of photochemistry in boreal biomass burning plumes have also been performed to evaluate ozone production and loss. Mauzerall et al. (1996) performed 1-D model simulations to calculate in situ production and loss of ozone based on the ABLE 3B measurements in the summer of 1990. They found biomass burning emissions to be a relatively negligible term contributing less than 2 % to the calculated ozone budget. McKeen et al. (2002) used a 3-D chemistry transport model (CTM) to evaluate the influence of Canadian biomass burning emissions on ozone production over the Northeastern USA using measurements made from the National Oceanographic and Atmospheric Administration (NOAA) WP-3 aircraft in the summer of 1995. Ozone enhancements of between 10 and 30 ppbv throughout the central and eastern US were attributed to the fires, with the model simulations being sensitive to NO_x/CO and VOC/CO emission ratios. The influence of emissions from forest fires in Alaska and Canada on tropospheric ozone production during summer 2004 was the subject of model studies by Pfister et al. (2006); Real et al. (2007); Cook et al. (2007). Pfister et al. (2006) utilised the MOZART-4 CTM to evaluate ozone production in the outflow from fires in Alaska during summer of 2004 with measurements made from aircraft during the ICARTT campaign and at the Pico Mountain Observatory and reported ozone enhancements relative to CO of 0.25 ppbv ppbv^{-1} and contributed approximately 3 % of the Northern Hemispheric tropospheric ozone budget. Lagrangian model studies of the outflow over the North Atlantic Ocean (Real et al., 2007) reported that although an ozone enhancement of 17 ppbv was observed after 5 days, net ozone loss could occur in the plumes due to biomass burning aerosols in the plume reducing the photolysis rates of O_3 and NO_2.

An overview of observed and model estimates of ozone production in boreal biomass burning plumes was recently presented by Jaffe and Wigder (2012). A common feature of observation and model studies of ozone production in biomass burning outflow is the use of ozone enhancement ratios relative to CO ($\Delta O_3/\Delta CO$) to determine ozone production. Jaffe and Wigder (2012) broadly showed that the $\Delta O_3/\Delta CO$ ratio increases with plume age. In this paper we evaluate ozone production in biomass burning plumes sampled over Eastern Canada using a number of different metrics, including $\Delta O_3/\Delta CO$, determined from measurements made from the BAe-146 research aircraft the BORTAS-B campaign in the summer of 2011. An overview of the measurements and chemical processes influencing ozone photochemistry are presented in Sect. 2. Section 3 presents the ozone distribution over Eastern Canada observed by the aircraft over the campaign period. Section 4 presents an analysis of observed plume photochemistry using photochemical age calculations derived from hydrocarbon ratios, ozone production efficiencies relative to NO_y partitioning, and photostationary steady state calculations. We conclude in Sect. 5.

2 Airborne photochemical measurements during BORTAS-B

In this section we present a brief overview of tropospheric ozone photochemistry and the relevant measurements made from the BAe-146 aircraft during the BORTAS-B aircraft measurement campaign and used in our analysis.

2.1 Plume photochemistry

The simplest model of ozone photochemistry in the atmosphere can be represented by the rapid oxidation of nitrogen oxides, NO_x, which represents the sum of nitric oxide (NO) and nitrogen dioxide (NO_2), in the presence of sunlight through the following null cycle:

$$NO + O_3 \rightarrow NO_2 + O_2 \tag{R1}$$

$$NO_2 + h\nu \rightarrow NO + O \tag{R2}$$

$$O + O_2 \xrightarrow{M} O_3 \tag{R3}$$

In polluted air masses such as biomass burning plumes, perturbations of this cycle through additional reactions of NO with peroxy radicals (RO_2 or HO_2) produced by the oxidation of VOCs provide additional pathways for converting NO_x into ozone. Figure 1 shows a schematic of the simplified ozone-NO_x-VOC chemistry in the atmosphere. The chain of reactions leading to ozone formation is initiated by the photo-oxidation of a VOC (RH) and its rapid subsequent reaction with molecular oxygen to produce alkyl peroxy radicals (RO_2), for example:

$$RH + OH \xrightarrow{O_2} RO_2 + H_2O \tag{R4}$$

Under tropospheric conditions, and following the blue arrows in Fig. 1, alkyl peroxy radicals can react with NO_2 via a three body reaction to form peroxynitrates (RO_2NO_2):

$$RO_2 + NO_2 \xrightarrow{M} RO_2NO_2 \tag{R5}$$

which will decompose back into the constituent RO_2 and NO_2 under the right environmental conditions (i.e. near surface temperatures) but can also be subject to transport away from the source region as they are thermally stable at lower temperatures, such as those in the free troposphere.

Peroxy radicals are also subject to reaction with NO and can follow two different pathways:

$$RO_2 + NO \rightarrow RO + NO_2 \tag{R6a}$$

$$RO_2 + NO \xrightarrow{M} RONO_2 \tag{R6b}$$

Reaction (R6a) results in the formation of ozone molecules via photolysis of NO_2. Comparison of Reaction (R6a, b) indicate that ozone production in biomass burning plumes initiated by photo-oxidation of VOCs is in competition with production of alkyl nitrates ($RONO_2$) and evaluating the relationship between the measured ozone and $RONO_2$ mixing ratios provides an indication of the potential for ozone production related to the above mechanism (e.g. Perring et al., 2010).

The potential of the above reactions to produce ozone in biomass burning plumes is dependent on the availability of nitrogen oxides, NO_x

(= NO + NO_2). A surrogate species, NO_y, is used to represent the sum of all reactive and oxidised nitrogen species in an air mass: $NO_y = NO_x + \Sigma RO_2NO_{2i} + \Sigma RONO_{2i} + HNO_3 + HONO + NO_3 + 2N_2O_5 + NO_3^-$, where ΣRO_2NO_{2i} represents the total peroxynitrates (ΣPN) and $\Sigma RONO_{2i}$ represents the total alkyl nitrates (ΣAN) (e.g. Day et al., 2003). A second surrogate species, NO_z (= $NO_y - NO_x$), can be defined that represents the sum of the photo-oxidation products of NO_x (Olszyna et al., 1994). Since NO_y is representative of all NO_x emissions, NO_z provides a measure of the number of NO_x molecules that have undergone photo-oxidation. Several studies have shown that ozone abundance in polluted air masses is linearly related to the abundance of NO_z (e.g. Trainer et al., 1993; Kleinman, 2000). The enhancement of ozone abundance relative to NO_z (i.e. $\Delta O_3/\Delta NO_z$) provides a measure of ozone production related to photo-oxidation of NO_x molecules, sometimes referred to as the ozone production efficiency (Rickard et al., 2002).

2.2 BORTAS measurements

Measurements of the key tracers relevant to the ozone photochemistry outlined above were made from the BAe-146 aircraft over the course of the BORTAS-B measurement campaign. Full details of the BAe-146 payload is presented by Palmer et al. (2012) and we provide brief details of the measurements used in this study.

Measurements of ozone were made using a TECO 49 ultraviolet absorption instrument (Wilson and Birks, 2006) operated by the UK Facility for Airborne Atmospheric Measurements (FAAM) with an averaging time of 3 Hz at a precision of 1 ppbv and accuracy of ± 5 %. Measurements used for identification of biomass burning plume air masses included acetonitrile (CH_3CN) and CO. A Proton Transfer Reaction Mass Spectrometer (PTR-MS) (Murphy et al., 2010) provided measurements of CH_3CN with an averaging time of 1 s and mean precision of 37 pptv over all BORTAS flights. CO was measured using a vacuum-UV resonance fluorescence instrument (Gerbig et al., 1999) with an averaging time of 1 s, precision of 1 ppbv, and accuracy of 3 %. We determine the aerosol loading within the sampled plume air with measurements of refractory black carbon using a single particle soot photometer (SP2) and measurements of total scattering coefficient at 550 nm using a TSI Inc. 3563 three-wavelength nephelometer (Anderson and Ogren, 1998). The SP2 uses laser-induced incandescence to measure refractory black carbon on a single particle basis (Schwarz et al., 2006) and the inlet and instrumental setup on the BAe-146 are described by McMeeking et al. (2010). The statistical uncertainty in BC mass concentration was 5 % for an averaging time of 15 s, and accuracy within 20 % due to possible differences between the instrumental response to biomass burning BC and the calibrant (Laborde et al., 2012). Measurement of NO_2 photolysis rates were made using upper and lower fixed bandwidth radiometers at wavelengths predominantly between 208 and 500 nm at a frequency of 1 Hz and with accuracy of 10 % (Volz-Thomas et al., 1996). Measurements of VOCs used in this study were made using a dual channel gas chromatograph system with flame ionisation detection (GC-FID) (Hopkins et al., 2003, 2011) to analyse whole air canister samples taken during each flight. Each canister sample was taken over a 30 s period at points of particular interest along the flight track. The precision and accuracy of the GC-FID measurements are species dependent but typical values are 1–5 pptv and 5 %, respectively. Measurements of NO and NO_2 were made using a single channel chemiluminesence instrument manufactured by Air Quality Design (AQD) Inc., USA. as described by Lee et al. (2009). Measurements of NO_2, total NO_y, total peroxyacetyl nitrates ($\Sigma PN = \Sigma RO_2NO_{2i}$), and total alkyl nitrates ($\Sigma AN = \Sigma RONO_{2i}$) were made using a Thermal Dissociation–Laser Induced Fluorescence (TD–LIF) instrument (Dari-Salisburgo et al., 2009; Di Carlo et al., 2012) with precisions of 10 %, 22 %, 34 %, and 46 % respectively.

We use mixing ratios of NO_x and NO_z calculated from aircraft measurements NO, NO_2 and NO_y described above. NO_x was calculated using NO measured by the AQD instrument and NO_2 from the LIF instrument. Although NO_2 was also measured by the AQD instrument, issues related to the detection limit of these measurements led to limited data availability and we chose to the use the LIF measurements. NO_z was then calculated by subtracting the AQD/LIF NO_x values from the LIF total NO_y measurements.

To distinguish measurements made in biomass burning plumes from those made in clean air, we use the threshold of 150 pptv of acetonitrile (CH_3CN) determined by Palmer et al. (2012) from the 99th percentile of measurements made on fight B625. Acetonitrile is predominantly emitted from biomass burning and removed from the atmosphere through uptake by the oceans and reaction with OH, with an atmospheric lifetime of approximately 25 days (Bange and Williams, 2000) and is, therefore, an excellent tracer for identifying plume measurements.

3 Observed ozone distribution over Eastern Canada

In this section we present an overview of the ozone distribution observed from the BAe-146 aircraft during the BORTAS-B measurement campaign. Figure 2 shows the relative frequency distribution of ozone mixing ratios, divided into 1 ppbv bins, measured from the BAe-146 during the eleven research flights undertaken between 15–31 July 2011 listed in Tables 1 and 2. The frequency distribution of the ozone measurements made both in and out of biomass burning plumes shows two peaks at approximately 25 and 50 ppbv. The peak in ozone mixing ratio at 25 ppbv is attributable to measurements made at altitudes below 3 km. The ozone measurements made during BORTAS-B show a similar distribution to that observed over central and Eastern Canada during the ABLE 3B measurement campaign in the summer of 1990 (Anderson et al., 1994).

Figure 3 summarizes the temporal and spatial distribution of the tropospheric ozone distribution over the campaign period. Table 1 lists the date and location of each research flight shown in Fig. 3. Boreal biomass burning plumes from different fire source regions were sampled by the BAe-146 throughout the BORTAS measurement campaign. Widespread fires in Northwestern Ontario burned between 17–19 July with episodic fire activity later in the campaign. Flights B621 on 18 July, B622 and B623 on 20 July, and B624 on 21 July intercepted the outflow from these fires approximately

1000–3000 km downwind of the source region. Flight B621 took place over two segments, making measurements between Halifax and Goose Bay NL via the Island of Newfoundland and Goose Bay and Halifax via the western edge of the Gulf of St. Lawrence. On the first segment a large range of ozone mixing ratios was measured throughout the free troposphere between 2 and 8 km with values ranging from about 20 ppbv to in excess of 100 ppbv with an average mixing ratio of 66.8 ± 18.0 ppbv. Plume air was sampled at all altitudes over Nova Scotia and the Island of Newfoundland with an average ozone mixing ratio of 68.2 ± 15.3 ppbv. Lower ozone mixing ratios were measured on the second segment with an average value of 47.3 ± 9.6 ppbv. Plume air was only sampled on this segment towards the end of the flight over Nova Scotia at altitudes around 2 km with an average ozone mixing ratio of 43.5 ± 12.1 ppbv. Flights B622 and B623 extended over a geographical region from 79° W in western Quebec across New Brunswick to approximately 62° W over Nova Scotia, sampling outflow from forest fires in Northwestern Ontario. Measurements were made throughout the free troposphere on these flights at altitudes between 2 and 8 km. Ozone mixing ratios measured on both flights were relatively invariant along the aircraft trajectories with an average value of 48.0 ± 7.0 ppbv. Biomass burning plume air was sampled throughout both research flights at all aircraft altitudes with an average ozone mixing ratio of 48.2 ± 6.3 ppbv. Flight B624 also sampled outflow from these fires at lower altitudes (2–3 km) over the Atlantic Ocean off the east coast of the Island of Newfoundland to a longitude of 51° W. Ozone mixing ratios measured on the first segment of this flight were higher on average than on the previous two flights at 54.8 ± 7.5 ppbv. Plume air was sampled extensively over the first flight segment with a slightly lower average ozone mixing ratio of 52.7 ± 6.9 ppbv. The second segment of flight B624 was a transit flight between St. John's NL and Halifax following a refuelling stop. Ozone mixing ratios measured on this segment were higher on average than the first segment, with an average value of 58.8 ± 5.5 ppbv.

Flight B626, on 26 July, was made over Northwestern Ontario to sample fresh biomass burning plumes. These measurements were made several days after the main fires had been burning but substantial localised enhancements of CO and other species associated with biomass burning were observed during the flight. The flight was made over two segments the first of which was a transit flight at altitudes above 7 km between Halifax NS and Thunder Bay ON. Ozone mixing ratios measured on this first flight section show a high degree of variability ranging from 21.5 ppbv to 101.4 ppbv. The second segment of the flight, at generally low altitudes (between 1 and 2 km) over Northwestern Ontario, observed relatively low ozone mixing ratios with an average value of 31.3 ± 9.4 ppbv.

The final three research flights, B628 on 28 July, B629 and B630 on 31 July, of the BORTAS campaign were made over the east coast of Canada with back trajectories, not shown, placing the source of the sampled outflow to fires in the vicinity of Great Slave Lake in the Northwest Territories. Flight B628 was made over two segments out of Goose Bay NL: the first segment, over the Atlantic Ocean off the east coast of Labrador, measured ozone mixing ratios between 26.2 and 119.1 ppbv with an average of 49.7 ± 16.5 ppbv; the second segment was a transit flight from Goose Bay to Halifax and measured average ozone mixing ratios of 47.2 ± 10.6 ppbv for all data and 51.1 ± 7.4 ppbv for the plume measurements. Flights B629 and B630 were made over the Gulf of St. Lawrence north of Nova Scotia and over the west coast of the Island of Newfoundland, respectively. In general, measurements from these two flights were made at relatively high altitudes between 6 and 8 km. Average ozone mixing ratios measured on these flights were higher than those measured on other flights during the campaign with mean values of 59.1 ± 12.7 ppbv for fight B629 and 59.6 ± 13.1 ppbv for flight B630. Plume air was sampled throughout both flights at altitudes above 5 km and the ozone mixing ratios in these air masses was 62.2 ± 6.7 ppbv and 65.2 ± 10.2 ppbv.

Flights B620 on 15 July, B625 on 24 July, and B627 on 27 July are not analysed in the context of the flights that intercepted biomass burning plumes from the fires in Northwestern Ontario and Northwest Territories due to limited measurements of species associated with biomass burning. Flight B620 did not measure acetonitrile although slight enhancements in CO, not shown, were observed at altitudes above

4 km. The average ozone mixing ratio on flight B620 was 50.0 ± 12.7 ppbv with ozone mixing ratios of approximately 40–55 ppbv associated with enhanced CO. Flight B625 was unusual in that measurements were made in mainly unpolluted air. Measured ozone mixing ratios on this flight showed a large range of values between 21.1 and 124.8 ppbv and exhibited a clear dependence on altitude with a correlation coefficient, $r = 0.86$. Flight B627 was a direct transit flight at altitudes above 7 km between Thunder Bay and Goose Bay. The measured ozone mixing ratios on this flight showed higher variability initially, with values ranging from 45 to 95 ppbv, which became lower, values in the range 45 to 60 ppbv, at the eastern end of the flight track.

Figure 4 shows a box and whisker plot of the distribution of measured ozone mixing ratios on each research flight. The data have been partitioned by an arbitrarily chosen planetary boundary layer (PBL) height of 2 km. Statistics (mean, median, standard deviation, and range of values) for each flight are given in Table 2. In the free troposphere, i.e. aircraft altitudes above 2 km, the mean and median ozone mixing ratios for each flight are distributed around the campaign mean of 54 ppbv within a range of 46 and 61 ppbv. The measurements made in the PBL are not uniformly distributed over the duration of the campaign period and can be separated into two distinct populations representing the first (flights B620 to B624) and second (flights B625 to B630) halves of the campaign. In the first half of the campaign average values in excess of 40 ppbv are observed comparable to the average values in the free troposphere with average values less than 35 ppbv over the second half (i.e. flights B625 to B630) and showing a clear partitioning between the PBL and FT measurements. It should be noted that of the measurements made in the PBL over the second half of the campaign, those on flights B627 through to B630 were only made during take off and landing while more extensive measurements were made in the PBL on flights B625 and B626. Figure 4b shows the box and whisker plot for measurements determined to be in biomass burning plumes using the acetonitrile threshold. The plume measurements show similar distributions to those for all measurements made in the first half of the campaign apart from B621, reflecting that plume air was measured throughout the duration of each flight.

Flight B621 shows a higher average plume ozone mixing ratio compared to all the data due to the flight being made over two legs with plume air sampled mostly on the first leg where the measured ozone mixing ratios were generally higher as shown in Fig. 3.

4 Observed boreal biomass burning outflow

In this section we evaluate the processes influencing the ozone distribution in biomass burning plume air sampled by the BAe-146 over the course of the BORTAS campaign. Figure 5 shows the relative distributions of 60-s averaged ozone and CO mixing ratios measured from the aircraft. As shown by Fig. 2, there is no discernible difference between ozone measurements made in the plume air to those in clean air. CO mixing ratios in plumes range from 64 to 930 ppbv. For CO mixing ratios in excess of 300 ppbv, ozone mixing ratios lie within a range between approximately 40 and 60 ppbv. In the following sub-sections we examine ozone production and photochemistry measured in boreal biomass burning plumes.

4.1 Photochemical ageing of biomass burning plumes

First, we investigate photochemical processing within biomass burning plumes sampled by the aircraft by calculating a photochemical age, i.e. the time taken for a particular measured tracer to be removed chemically from an air mass since emission. We calculate photochemical ages based on ratios of non-methane hydrocarbons (NMHCs) (Parrish et al., 2007), and the lightest alkanes (ethane, propane and *n*-butane) in particular, measured by GC-FID from whole air canister samples taken over the course of the BORTAS campaign. Figure 6 shows the relationship between natural logarithms of ratios of the observed mixing ratios of *n*-butane : ethane and propane : ethane. The ratio of initial mixing ratios for each NMHC pair, shown as the green square in Fig. 6, are determined from flight B626 over Northwestern Ontario on 26 July which was the main source of biomass burning early in the campaign with fires burning from 17–19 July. We assume that the higher values of the natural logarithm of the NMHC ratios from flight B626 are representative of the ratios of fresh emissions of these NMHCs. In general, the NMHC ratios measured in biomass burning plumes during BORTAS lie to the left and below this point indicating that the estimated initial concentrations are a suitable reference point for calculating the relative photochemical ageing of the biomass burning plumes sampled during the campaign. The red solid lines originating from the initial concentration ratios are the kinetic and mixing slopes. The kinetic slope is the steeper of the two and represents the relationship between the NMHC pairs if oxidation by OH was the only process affecting their behaviour. The mixing slope represents the relationship between the NMHC pairs if the only process was mixing of fresh emissions with background air. Most of the measured NMHC ratios lie between these two lines indicating that the sampled air masses experiened a combination of oxidation and mixing processes. The kinetic slope of the plotted NMHC ratios was calculated for kinetic reaction rate coefficients of the alkanes with OH at a temperature of 273 K, taken from Atkinson and Arey (2003), has a gradient of 2.61. The gradient of the line of best fit to the data is 1.55 further indicating that the observations were subject to mixing and photochemical processing. Outliers in Fig. 6, i.e. where $\ln([\text{propane}]/[\text{ethane}]) > -1$ and $\ln([n\text{-butane}]/[\text{ethane}]) > -2$, show measurements representative of different emission sources and are beyond the scope of the work presented here.

In general, NMHC ratios measured during BORTAS lie between −3 and −1 for ln([propane]/[ethane]) and between −6 and −2.5 for ln([*n*-butane]/[ethane]) and are consistent with previous observations of NMHC ratios (Rudolph and Johnen, 1990; Parrish et al., 1992; Jobson et al., 1994; Parrish et al., 2007; Helmig et al., 2008). We estimate plume ages in days for the plume air masses sampled during the BORTAS campaign using the ln(propane/ethane) ratio and assuming an average summertime OH concentration at Northern Hemisphere mid-latitudes of 2×10^6 molecules cm^{-3} (Spivakovsky et al., 2000). Estimating photochemical ages in this way allows us to compare ozone production in boreal biomass burning plumes measured over the BORTAS campaign to similar measurements used in previous studies.

4.2 Ozone enhancements in biomass burning plumes

Figure 7 shows the relationships between ozone and CO measured in biomass burning plumes during the BORTAS measurement campaign to the calculated photochemical ages, sampled at the times of the whole air canister samples. Ozone mixing ratios measured in boreal biomass burning plumes, Fig. 7a, show no clear relationship to the calculated photochemical age over the whole BORTAS campaign period. The ozone measurements made on flight B626 are distinguished from those made on the other research flights by mixing ratios less than 30 ppbv. It should be noted that the measurements made in biomass burning plumes on flight B626 were made at lower altitudes (below 1.5 km) than on other flights as shown in Figs. 2 and 4. Measurements with higher acetonitrile mixing ratios typically show moderate ozone mixing ratios between 40 and 70 ppbv with photochemical ages between 1.5 and 4.5 days. The measurements made with lower acetonitrile exhibit a wider range of ozone mixing ratios, from 40 to 110 ppbv, and photochemical ages, from 0 to 15 days. The CO mixing ratios measured in boreal biomass burning plumes, Fig. 7b, typically show higher values (between 200 and 1100 ppbv) at photochemical ages of between 2 and 4 days and are coincident with the higher values of acetonitrile. These measurements were made at aircraft altitudes below 3 km during flights B622–B624 on 20 and 21 July in plumes from the fires in Northwestern Ontario with approximate transport times of 2–3 days, calculated by Langrangian backward trajectories (not shown). Measurements of CO mixing ratios less than 200 ppbv have a wider range of photochemical ages, between 0 and 15 days. On flight B626, CO mixing ratios were measured between 150 and 400 ppbv with photochemical ages from 0 to 8.5 days.

The relationship between the measured ozone and CO mixing ratios in boreal biomass burning plumes is shown in Fig. 7c for the data sampled at the times of the whole air canister samples. The distribution is similar to that shown by the red symbols in Fig. 5 for the 60-s averaged data. The three populations of data points defined for flight B626, and moderate and high acetonitrile show clear distinctions from one another. Straight lines fitted to each population and their slopes provide an indication of ozone produced since the fire emissions of CO and other precursors at the source, i.e. $\Delta O_3/\Delta CO$ (Parrish et al., 1993; Pfister et al., 2006). Measurements of fresh biomass burning air masses were made during flight B626, indicated by a slope of 0.009 ppbv ppbv^{-1}. Of the measurements made on the other BORTAS research flights, those with the highest acetonitrile mixing ratios were made in moderately fresh plume air masses with photochemical ages of 2–4 days. The gradient of the straight line fitted to these data points is 0.016 ppbv ppbv^{-1} suggesting a slight increase in ozone production downwind of the emission source. Measurements with moderate acetonitrile are typically more aged (photochemical ages $>$ 4 days) and indicate increased ozone production relative to the other two populations, as reflected in the gradient of the straight line fitted to these data points of 1.29 ppbv ppbv^{-1}. Figure 5d shows enhancement ratios of ozone relative to CO as a function of photochemical age. Enhancements of ozone and CO (i.e. ΔO_3 and ΔCO) are calculated relative to background values determined from the 25th percentile of the distribution of clean air measurements (i.e. acetonitrile mixing ratios less than 150 pptv). Background values of ozone and CO were calculated to be 33 ppbv (24 ppbv for flight B626) and 60 ppbv, respectively. The $\Delta O_3/\Delta CO$ ratios for the three populations of data show a similar trend to the gradients calculated for the ozone to CO relationship in Fig. 5c with the value of $\Delta O_3/\Delta CO$ increasing from the measurements made on flight B626 through the high acetonitrile measurements to the moderate acetonitrile measurements. The measurements made on flight B626 have $\Delta O_3/\Delta CO$ ratios between approximately 0.015 and 0.05 ppbv ppbv^{-1} over a range of photochemical ages between 0 and 8 days. The $\Delta O_3/\Delta CO$ ratio decreases from 0.03 to 0.01 ppbv ppbv^{-1} between 0–2 days of photochemical ageing, with the lowest values associated with higher CO mixing ratios of in excess of 250 ppbv, increasing from approximately 150 ppbv (Fig. 7b), and increases from 0.03 to 0.05 ppbv ppbv^{-1} between 5–8 days of photochemical ageing.

The high acetonitrile measurements show a wide range of $\Delta O_3/\Delta CO$ ratios, from 0.02 to 0.3 ppbv ppbv^{-1}, between 2–4 days of photochemical ageing. A few high acetonitrile measurements with photochemical ages between 4 and 8 days have higher $\Delta O_3/\Delta CO$ ratios from 0.2–0.5 ppbv ppbv^{-1}. In general the moderate acetonitrile measurements have photochemical ages greater than 4 days and exhibit higher $\Delta O_3/\Delta CO$ ratios between 0.1 and 1.0 ppbv ppbv^{-1}. Some measurements with moderate acetonitrile have photochemical ages less than 4 days although this does not appear to significantly affect the $\Delta O_3/\Delta CO$ ratio in these air masses. The measurements made with less than 2 days photochemical ageing and $\Delta O_3/\Delta CO$ ratios greater than 0.07 ppbv ppbv^{-1} may be attributable to a fire source with different initial NMHC mixing ratios to those used in the photochemical age calculation or could be aged air masses that have experienced mixing with air of different origin which has influenced the NMHC abundance. Further analysis of these data points is beyond the scope of the analysis presented here.

A review of ozone production in the outflow from wildfires, including boreal regions, was recently presented by Jaffe and Wigder (2012). Table 3 presents statistics of $\Delta O_3/\Delta CO$ ratios in boreal biomass burning plumes sampled during BORTAS arranged by photochemical age following Jaffe and Wigder (2012). The BORTAS results show that the $\Delta O_3/\Delta CO$ ratio increases with plume age in both the range and average (mean and median) values indicating that ozone production is enhanced in plumes that have undergone more photochemical processing as they are transported away from the source region. For plume ages less than 2 days the BORTAS $\Delta O_3/\Delta CO$ ratios are within the range of ARCTAS measurements for the same category (Alvarado et al., 2010) and the mean BORTAS value of 0.020 ppbv is comparable to the mean of 0.018 ppbv calculated by Jaffe and Wigder (2012) from studies by Alvarado et al. (2010); Goode et al. (2000); Singh et al. (2010); DeBell et al. (2004). For plume ages between 2 and 5 days the range of BORTAS $\Delta O_3/\Delta CO$ ratios are comparable to the ranges determined for boreal biomass burning plumes from Eastern Canada (Mauzerall et al., 1996) and Siberia (Tanimoto et al., 2008). The average $\Delta O_3/\Delta CO$ ratio of 0.15 ppbv ppbv^{-1} calculated by Jaffe and Wigder (2012) for this plume category is double the mean of 0.07 ppbv ppbv^{-1} calculated for the high acetonitrile measurements taken over the BORTAS campaign but is more comparable to the increased mean of 0.21 ppbv ppbv^{-1} when the moderate acetonitrile measurements are included, although it should be noted that the range including these measurements is greater than the range reported in Jaffe and Wigder (2012). For plume ages greater than 5 days the BORTAS $\Delta O_3/\Delta CO$ ratios are typically within the range of values presented by Jaffe and Wigder (2012). The mean $\Delta O_3/\Delta CO$ ratio of 0.66 ppbv ppbv^{-1} for BORTAS is higher than the mean values of approximately 0.25 ppbv ppbv^{-1} for North American boreal biomass burning plumes (Pfister et al., 2006; Val Martin et al., 2006) and is more comparable to similarly aged plumes originating in Siberia (Bertschi and Jaffe, 2005; Honrath et al., 2004). The upper-limit of 3.00 ppbv ppbv^{-1} in the range of $\Delta O_3/\Delta CO$ ratios for these measurements is much higher than for the data presented by Jaffe and Wigder (2012). Restricting this upper-limit removes two data points from the BORTAS statistics, reducing the mean value from 0.63 to 0.55 ppbv ppbv^{-1} and the standard deviation from 0.52 to 0.29 ppbv ppbv^{-1}.

4.3 Ozone photochemistry in boreal biomass burning outflow

The $\Delta O_3/\Delta CO$ ratios presented above assume that enhancements in plume air over background values provide an indication of ozone production in biomass burning plumes. However, this ratio provides limited information on the photochemistry occurring in the plume air masses. We now evaluate ozone mixing ratios measured in boreal biomass burning plumes during the BORTAS campaign against measurements of other chemical species associated with ozone photochemistry.

4.3.1 Ozone production efficiency

We evaluate the ozone production efficiency in the plumes sampled during the BORTAS campaign through comparison of the measured ozone mixing ratios to measurements of alkyl nitrates and the surrogate species NO_z. Photochemical production of ozone in polluted air masses is dependent on the interaction between VOC and NO_x chemistry as shown in Fig. 1 and Reactions (R4–R6a, b). Thus, comparing the products of Reaction (R6a, b) provides an indication of the potential for ozone production in an air mass based on the relative concentrations of alkyl nitrates ($RONO_2$ in Reaction (R6a, b) and referred to as ΣAN from hereon in) and odd oxygen ($O_x = O_3 + NO_2$). The distribution of O_x relative to ΣAN measured in boreal biomass burning plumes during BORTAS, Fig. 8a, shows three main populations of data points with a distinctive "L-shape" distribution for measurements made on all BORTAS research flights not including flight B626 (i.e. O_x mixing ratios in excess of 30 ppbv). Higher values of ΣAN generally correspond to lower values of O_x, and lower values of ΣAN generally correspond to higher values of O_x. High aerosol loading in the plumes is determined using measured black carbon mass concentration greater than 0.1 $\mu g\,cm^{-3}$ and nephelometer measurements of the total scatter coefficient at 550 nm greater than $1.1 \times 10^{-5}\,m^{-1}$ (corresponding to a black carbon mass concentration of 0.1 $\mu g\,cm^{-3}$, and used to fill in gaps in the black carbon measurements). Although the vast majority of scattering is due to nonrefractory aerosols, the black carbon mass concentration and total scatter coefficient measurements are strongly correlated ($r = 0.92$) in the biomass burning plumes sampled during BORTAS and indicates that these are reliable indicators of plume aerosol loading. The highest mixing ratios of ΣAN (> 0.5 ppbv) were measured at nighttime with corresponding O_x mixing ratios between approximately 40 and 60 ppbv. Daytime measurements along the horizontal branch of the "L-shape" distribution were typically made in air masses with high aerosol loading and a wide range of ΣAN and O_x, between 0–0.5 ppbv and 40 and 60 ppbv, respectively. Nighttime measurements along this branch of the distribution show a wider range of ΣAN, between 0.05 and 0.8 ppbv with the same range of O_x mixing ratios as the daytime measurements. Data points along the vertical branch of the "L-shape" distribution show measurements made during daytime and nighttime, with daytime measurements showing low aerosol loading. The third population of data points, with O_x mixing ratios less than approximately 40 ppbv, corresponds to measurements made during flight B626 over Northwestern

Ontario and show a narrower range of O_x (25–30 ppbv) for ΣAN between 0.05 and 0.4 ppbv. The higher mixing ratios of ΣAN in this population (> 0.15 ppbv) were associated with high aerosol loading. Straight lines fitted using a non-linear least squares method to each population of data points in Fig. 8a provide an indication of the potential for ozone formation relative to ΣAN. For relatively fresh biomass burning plumes measured on flight B626 the slope of the fit is approximately 2 ppbv ppbv^{-1} (i.e. two O_x molecules are produced for every molecule of ΣAN). The gradient increases to approximately 8 ppbv ppbv^{-1} for the plume measurements with photochemical ages less than 4 days and with high aerosol loading, and approximately 473 ppbv ppbv^{-1} for the plume measurements with photochemical ages greater than 5 days and with low aerosol loading. The change in the relationship between O_x and ΣAN with plume photochemical age observed during BORTAS is consistent with that observed in pollution outflow from Mexico City by Perring et al. (2010) in which slopes of the lines of best fit to aircraft measurements in the outflow increased from approximately 16 ppbv ppbv^{-1} to 89 ppbv ppbv^{-1} as the plume age increased from less than 10 h to between 40 and 50 h.

Figure 8b shows the distribution of O_x relative to the surrogate species NO_z (= $NO_y - NO_x$), representing the photooxidation products of reactive nitrogen species (i.e. NO_x). The data are filtered for daytime/nighttime and aerosol loading as in Fig. 8a. As with Fig. 8a, the distribution of O_x relative to NO_z shows three main populations of data points with the measurements made on all BORTAS research flights other than flight B626 forming a distinctive "L-shape" distribution (O_x mixing ratios > 30 ppbv) with higher values of NO_z corresponding to lower O_x and lower values of NO_z corresponding to higher O_x. In this case, the highest values of NO_z (mixing ratios > 2 ppbv) were generally made during the daytime in plume air with high aerosol loading. Measurements made at nighttime in plume air with low aerosol loading generally have lower NO_z mixing ratios (< 2 ppbv) although a significant number of data points flagged as daytime and high black carbon have similar values of NO_z. The range of O_x mixing ratios corresponding to these values of NO_z is similar to those for the horizontal branch of the “L-shape” distribution in Fig. 8, i.e. between 40 and 60 ppbv. Measurements made with low aerosol loading lie along the vertical branch of the “L-shaped” distribution with NO_z mixing ratios between 0 and 0.5 ppbv and ozone mixing ratios between 40 and 90 ppbv. The third population, with O_x mixing ratios less than 30 ppbv corresponds to measurements made during flight B626 over Northwestern Ontario. These measurements show the same range of O_x mixing ratios as in Fig. 8 but with a smaller relative range of NO_z (0.1–0.5 ppbv) compared to the range of ΣAN. The slopes of straight lines fitted using a non-linear least squares method to the three populations of data points in Fig. 8b are consistent with the slopes calculated in Figs. 7d and 8a. The slopes of the change in O_x relative to the change in NO_z (i.e. the number of molecules of O_x formed per molecule of NO_x that undergoes photo-oxidation) are calculated to be 0.07 ppbv ppbv^{-1} for flight B626, 1.61 ppbv ppbv^{-1} for plume air with high aerosol loading, and 155.07 ppbv ppbv^{-1} for plume air with low aerosol loading. It should be noted that ozone production efficiency calculated in this way represents an upper limit due to potential loss of ozone and NO_y species from the plume air due to wet and dry deposition (e.g. Wang et al., 1996; Rickard et al., 2002).

The distribution of O_x relative to NO_z in Fig. 8b indicates a linear relationship for the different plume air masses and provides a measure of ozone production efficiency. The ratio of O_x and NO_z enhancements relative to background values (i.e. $\Delta O_x/\Delta NO_z$) are calculated from the BAe-146 measurements to indicate the ozone production efficiency for all data points throughout the BORTAS measurement campaign. Figure 9 shows the distribution of $\Delta O_x/\Delta NO_z$ ratios relative to NO_x mixing ratios in boreal biomass burning plumes. The measurements are filtered for daytime/nighttime and high/low aerosol loading as in Fig. 8. Measurements made in plume air with high aerosol loading (red closed diamonds in Fig. 9) typically have ozone production efficiencies less than 70 ppbv ppbv^{-1} with NO_x mixing ratios ranging from 0.05 and 0.6 ppbv. Measurements with low aerosol loading have higher ozone production efficiencies with $\Delta O_x/\Delta NO_z$ ratios between 50 and 400 ppbv ppbv^{-1} and a narrower range of NO_x mixing ratios between 0 and 0.25 ppbv. The NO_x mixing ratios in this branch of the distribution shows a clear distinction between higher (> 0.1 ppbv) and lower (< 0.1 ppbv) NO_x mixing ratios with higher values corresponding to the nighttime measurements. The measurements made on flight B626 over Northwestern Ontario have low ozone production efficiencies less than 30 ppbv ppbv^{-1} over a similar range of NO_x mixing ratios as the high aerosol measurements. The changes in ozone production efficiency relative to NO_x for the two populations of data points defined by the aerosol loading indicates that plume measurements were made under two different chemical regimes. For the measurements made on flight B626 and those made during daytime with high aerosol loading, the large range of NO_x mixing ratios and small change in the $\Delta O_x/\Delta NO_z$ ratio are indicative of a more VOC-limited regime. For the low aerosol loading measurements, the much narrower range of NO_x mixing ratio and larger change in the $\Delta O_x/\Delta NO_z$ ratio are indicative of a more NO_x-limited regime.

Figure 10 shows the distributions of relative humidity (RH) and aircraft altitude relative to the $\Delta O_x/\Delta NO_z$ ratio partitioned for nighttime/daytime and high/low aerosol loading as described above. Figure 10a shows that the measurements made with ozone production efficiency less than 70 ppbv ppbv^{-1} are typically characterised by higher relative humidity (> 40 %) than the measurements with ozone production efficiency higher than 70 ppbv ppbv^{-1} (RH typically < 40 %). The relationship between RH and the $\Delta O_x/\Delta NO_z$ ratio shows no distinction between daytime and nighttime measurements. Figure 10b shows vertical distribution of RH measured in boreal biomass burning plumes throughout the campaign. In general measurements with low aerosol loading and low RH were made at higher altitudes (> 3 km) during both daytime and nighttime. Interestingly, measurements with high aerosol loading and high RH but low ozone forming potential were not solely made at lower altitudes but across the entire vertical range of the measurements, from 0.5 to 7 km.

4.3.2 Photostationary steady state and instantaneous ozone production

To further evaluate ozone photochemistry in the biomass burning plumes sampled during the BORTAS campaign we use a photostationary steady state calculation to quantify the relative contributions of NO_x and other peroxy radicals to the ozone production efficiency. From Reactions (R1) and (R2) and assuming photostationary steady state (i.e. the loss of ozone via Reaction R1 is equal to the production of ozone via Reaction R2), the following ratio can be defined:

$$\Phi = \frac{j_{NO_2}[NO_2]}{k_{NO+O_3}[NO][O_3]} \quad (1)$$

where Φ is known as the photostationary ratio, [X] represents the concentration of species X, j_{NO_2} is the photolysis rate of NO_2 in units of s^{-1}, and k_{NO+O3} is the kinetic rate coefficient for the reaction between NO and O_3 in units of molecules $cm^{-3}\,s^{-1}$. The value of k_{NO+O_3} was calculated along the aircraft flight track using the recommended IUPAC definition of $1.4^{-12}\exp(-1310/T)$ (Atkinson et al., 2004) where T is the air temperature measured from the aircraft. The photostationary ratio would have a value of unity if chemical cycling between ozone and NO_x was the only process occurring (Leighton, 1961; Cantrell et al., 2003; Griffin et al., 2007). Deviations of this ratio from unity therefore give an indication of the influence of other chemical processes, for example, interaction between NO and families of organic peroxy radicals (RO_x) and hydro peroxy radicals (HO_x), we generalise these families of peroxy radicals as HO_xRO_x following Cantrell et al. (2003).

Figure 11 shows plots of photostationary steady state calculations made with the BORTAS aircraft measurements in biomass burning plumes over the course of the campaign. The photostationary ratio defined above is calculated from the measured values of each parameter in Eq. (1). Figure 11a shows the photostationary ratio versus NO_x mixing ratio with symbols denoting measurements made during daytime/nighttime and high/low aerosol as defined above. The calculated ratios for all the plume data points show a wide range of values between 0 and 10. Ratios for the measurements made at nighttime or with low aerosol loading generally lie in a narrower range from 0 to 2 indicating that the measurements are closer to photostationary steady state.

The measurements made during daytime and with high aerosol generally have photostationary ratios greater than 2 with a wide range of values extending as high as 10. Figure 11b also shows the calculated photostationary ratio but as a function of the ratio NO_x/NO_y. Note that the expression defining NO_z (i.e. $NO_z = NO_y - NO_x$) can be rewritten as $NO_z = NO_y(1 - NO_x/NO_y)$ in which the term $(1 - (NO_x/NO_y))$ can be considered as a measure of the photochemical age of the air mass (i.e. the fraction of the initial NO_x emitted that has been converted into photooxidation products, as NO_y represents total NO_x emissions) (Olszyna et al., 1994). Values of NO_x/NO_y closer to unity are therefore representative of fresher emissions because there has been less photochemical processing of NO_x. In general the BORTAS plume measurements have a range of NO_x/NO_y values between 0.0 and 0.4 indicating relatively aged air masses. This is perhaps not all that surprising given that the majority of the BORTAS measurements were made downwind of biomass burning source regions in Central Canada. The data points in Fig. 11 with NO_x/NO_y values greater than 0.4 are measurements made on flight B626 over Northwestern Ontario indicating that fresher air masses were encountered closer to one of the main source regions. The measure of air mass photochemical age from the ratio of NO_x/NO_y is shown relative to the surrogate species NO_z in Fig. 11c. Measurements with NO_z mixing ratios less than 1 ppbv were made in both fresh and aged plumes with the fresher plumes ($NO_x/NO_y > 0.4$) all having higher aerosol loading. Measurements with NO_z mixing ratios greater than 1 ppbv were all made in aged plumes ($NO_x/NO_y < 0.2$).

Using the measurements used to calculate the photostationary ratio, and including an additional term for the reaction of NO with peroxy radicals in Eq. (1) (Cantrell et al., 2003; Griffin et al., 2007) a photostationary ratio $\Phi_{HO_xRO_x}$ can be defined:

$$\Phi_{HO_xRO_x} = \frac{j_{NO_2}[NO_2]}{k_{NO+O_3}[NO][O_3] + k_{NO+HO_2}[NO][HO_xRO_x]} \tag{2}$$

where k_{NO+HO_2} is the kinetic rate coefficient for the reaction between NO and HO_2, calculated along the aircraft flight track using the recommended IUPAC definition of

$3.6^{-12}\exp(270/T)$ (Atkinson et al., 2004). Assuming photostationary steady state, we estimate mixing ratios of HO_xRO_x required to bring the photostationary ratio to unity by rearranging Eq. (2):

$$[HO_xRO_x] = \frac{j_{NO_2}[NO_2]}{k_{NO+HO_2}[NO]} - \frac{k_{NO+O_3}[O_3]}{k_{NO+HO_2}} \quad (3)$$

Figure 11d shows the HO_xRO_x mixing ratios estimated from the BORTAS plume measurements using Eq. (3) versus the NO_x/NO_y ratio. The measurements that were closer to unity in Fig. 11a, b (i.e. nighttime or with low aerosol loading) generally show the lowest HO_xRO_x mixing ratios with values below 0.1 ppbv. For the daytime plume measurements with high aerosol loading the estimated HO_xRO_x mixing ratios are generally greater than 0.1 ppbv and extend up to approximately 0.4 ppbv. In the fresher plumes (i.e. $NO_x/NO_y > 0.4$) the HO_xRO_x mixing ratios are estimated to be just over 0.1 ppbv, with higher mixing ratios generally associated with more aged plumes. The calculated HO_xRO_x mixing ratios are consistent with those calculated for a ground-based rural measurement site in the Northeastern USA (Griffin et al., 2007).

4.3.3 Observed ozone chemistry on previous measurement campaigns

We put the BORTAS plume measurements into context through comparisons with previous aircraft measurement campaigns with a focus over the Central and Eastern Canada, and sampled outflow from boreal biomass burning. Measurements from two different campaigns are used for this contextual analysis: the NASA Arctic Research of the Composition of the troposphere from Aircraft and Satellites (ARCTAS) campaign during the summer of 2008 (Jacob et al., 2010); and the NASA Atmospheric Boundary Layer Experiment (ABLE 3B) campaign during the summer of 1990 (Harriss et al., 1994).

Figure 12 shows an evaluation of ozone production efficiency in boreal biomass burning plumes observed during the ARCTAS-B measurement campaign between 29

June and 13 July 2008. We use 60-s averaged measurements of ozone, NO, NO_2 and NO_y made by chemiluminescence (Weinheimer et al., 1994), CO made by Tunable Diode Laser Absorption Spectroscopy (TDLAS) (Sachse et al., 1987), acetonitrile made by PTR-MS (Wisthaler et al., 2002), and black carbon from SP2 (Moteki and Kondo, 2007; Kondo et al., 2011). For comparison against the BORTAS measurements, the ARCTAS-B data are filtered to cover a similar ranges of altitude (0.5–8.0 km), longitudes (110–50° W), and latitudes (40–60° N). The symbols in each plot are the same as those defined for the BORTAS data to distinguish between daytime/nighttime and low/high aerosol measurements. Plume measurements are determined as for the BORTAS measurements, with acetonitrile mixing ratios in excess of 150 pptv and high aerosol loading is determined for black carbon mass concentrations greater than $0.1\,\mu g\,cm^{-3}$. Figure 12a shows O_x mixing ratios versus NO_z mixing ratios measured in boreal biomass burning plumes over the ARCTAS-B campaign. Distinct populations of data points associated with high/low NO_z and low/high O_x, similar to those observed in the BORTAS measurements in Fig. 8b. As with the BORTAS measurements the data points in each of these populations can be distinguished based on the aerosol loading of the plume with low aerosol measurements at low NO_z mixing ratios (< 1.0 ppbv) and high aerosol measurements at higher NO_z mixing ratios. It should be noted from Fig. 12 that most of the ARCTAS measurements were made during the daytime. Figure 12b shows $\Delta O_x/\Delta NO_z$ enhancement ratios versus NO_x mixing ratios. Enhancements in O_x and NO_z are calculated relative to background values of 25 ppbv and 0.1 ppbv, respectively. The distribution of $\Delta O_x/\Delta NO_z$ ratios as a function of NO_x is similar to that observed for BORTAS in Fig. 9 with lower values of $\Delta O_x/\Delta NO_z$ (< 50 ppbv ppbv^{-1}) generally associated with higher values of NO_x (> 0.5 ppbv). Measurements of plume air with high aerosol loading are also shown to have higher ozone production efficiency consistent with the BORTAS measurements which exhibited a larger range of $\Delta O_x/\Delta NO_z$ up to 400 ppbv ppbv^{-1}, compared to 200 ppbv ppbv^{-1} for the ARCTAS-B measurements. Figure 12c shows the NO_x/NO_y ratios versus NO_z to indicate the range of airmass photochemical ages as described above. The ARCTAS-B range of NO_x/NO_y values is similar to those in Fig. 11c for BORTAS although it should be noted that ARCTAS-B made considerably more measurements in fresh plumes ($NO_x/NO_y > 0.4$) reflecting the more localised deployment of the ARCTAS-B measurements to biomass burning sources in Central Canada.

Figure 13 shows the relationship of ozone forming potentials from measurements made in polluted air masses during the ABLE 3B measurement campaign between 6 July and 15 August 1990. We use 90-s averaged measurements of ozone, NO, NO_2 and NO_y, CO, and carbon tetrachloride (C_2Cl_4) (Blake et al., 1994; Harriss et al., 1994; Sandholm et al., 1994; Wofsy et al., 1994). The ABLE 3B deployment was very similar to that of BORTAS with measurements extending from Northwest Territories and northern Manitoba across Ontario and Quebec to the east coast of Labrador. No acetonitrile measurements were made during ABLE 3B and plume measurements are determined from where measurements of carbon tetrachloride (C_2Cl_4) mixing ratios, a tracer of anthropogenic emissions (Wofsy et al., 1994) were below 20 pptv and CO mixing ratios were greater than 150 ppbv. The aerosol loading in the plume measurements are determined from concentrations of total fine (0.195–3.12 µm) and coarse (0.5–8.0 µm) particles greater than 20 cm^{-3}. The observed O_x distribution relative to NO_z for all ABLE 3B research flights is shown in Fig. 13a and is similar to the horizontal branches of the “L-shaped” distributions in the BORTAS and ARCTAS-B measurements (Figs. 8b and 12a) with a moderate range of O_x mixing ratios (70–80 ppbv) at higher NO_z mixing ratios (> 3 ppbv). The maximum O_x mixing ratio was less than 80 ppbv reflecting the relatively low altitudes (typically below 6 km) over which the ABLE 3B measurements were made. The $\Delta O_x/\Delta NO_z$ enhancement ratios in boreal biomass burning plumes during ABLE 3B show a relatively low ozone forming potential (less than 100 ppbv ppbv^{-1}) corresponding to NO_x mixing ratios between 0 and 0.2 ppbv, Fig. 13b, representative of moderately fresh plumes with high aerosol loading in the BORTAS data. NO_x/NO_y ratios calculated from the ABLE 3B measurements typically have values less than 0.2 ppbv ppbv^{-1} over a range of NO_z mixing ratios between 0.5 and 6 ppbv, Fig. 13c, indicate that the sampled plumes were not freshly emitted consistent with NO_x/NO_y

ratios in plumes with high aerosol loading and NO_z mixing ratios greater than 1 ppbv observed during BORTAS (Fig. 11c).

The relationship between ozone mixing ratio and the ozone production efficiency in boreal biomass burning plumes for the BORTAS, ARCTAS-B, and ABLE 3B measurement campaigns is shown in Fig. 14. The measurements with low ozone production efficiency, less than 80 ppbv ppbv^{-1}, show a range of ozone mixing ratios between 25 and 80 ppbv and show clear distinctions between the measurements made on the three campaigns. The lowest ozone mixing ratios (25–30 ppbv) were measured on BORTAS flight B626 and the ARCTAS-B measurements typically lie between these values and ozone mixing ratios measured on the other BORTAS flights which range from approximately 40–55 ppbv. The ABLE 3B measurements at these lower ozone production efficiencies have higher ozone mixing ratios, 55–80 ppbv, and may reflect ozone mixing ratios representative of aged plumes (NO_x/NO_y ratios < 0.1 ppbv ppbv^{-1} in Fig. 13c). Higher ozone mixing ratios, 50–80 ppbv, are observed for ozone production efficiencies between 80 and 180 ppbv ppbv^{-1} for the ARCTAS-B measurements, and greater than 100 ppbv ppbv^{-1} for the BORTAS measurements corresponding to aged plumes with NO_x/NO_y ratios < 0.2 ppbv ppbv^{-1} in Figs. 12c and 11c and low aerosol loading.

5 Conclusions

We have presented an analysis of ozone photochemistry in boreal biomass burning plumes from a synthesis of aircraft measurements made over Eastern Canada during July and August 2011 as part of the BORTAS measurement campaign. We evaluated the tropospheric ozone distribution observed over the course of the measurement campaign and the potential for quantifying the photochemical processes influence ozone production and loss within boreal biomass burning plumes. The range of the measured ozone mixing ratios was typically between 45 and 70 ppbv, based on the lower and upper quartiles of the measurements on each research flight. Over the campaign as a whole there was no distinguishable difference between ozone measurements made within plume and those made in clean air. At the highest values of CO (> 300 ppbv) we observed a relatively narrow range of ozone mixing ratios between approximately 40 and 60 ppbv. We evaluated photochemical processes influencing the observed ozone distribution using a number of different measurements made from the aircraft throughout the campaign. First, photochemical ageing of the plume measurements was determined using canister samples of different alkanes and their relationship to ozone enhancements relative to CO. Second, the relative contributions of photochemical cycling of NO_x and peroxy radicals was analysed assuming photochemical steady state.

We calculated photochemical ages of the measured plumes using ratios of different alkanes assuming a common sink through oxidation with OH (Parrish et al., 2007) and found values that were consistent with previous measurements of biomass burning plumes. We used these ratios to estimate that plumes sampled during the campaign ranged in age from 0 to 15 days. When biomass burning plume measurements were evaluated relative to these estimated ages we found that the highest measured values at ages of 2–3 days and distances of 1000–3000 km from the expected emissions sources and reflected the transport time of the plume to where it was intercepted by the aircraft. We calculated ozone production in boreal biomass burning plumes, using $\Delta O_3/\Delta CO$ enhancement ratios, to be $0.020 \pm 0.008\ \mathrm{ppbv\,ppbv^{-1}}$ for plume ages less than 2 days which increased to $0.12 \pm 0.07\ \mathrm{ppbv\,ppbv^{-1}}$ for plume ages between 2 and 5 days, and $0.55 \pm 0.29\ \mathrm{ppbv\,ppbv^{-1}}$ for plume ages greater than 5 days. The increase in plume ozone production with photochemical age was consistent with a recent review of ozone production in boreal biomass burning outflow (Jaffe and Wigder, 2012).

We also performed a detailed analysis of the photochemical processes influencing the ozone distribution in boreal biomass burning plumes using measurements of total alkyl nitrates (ΣAN), NO_x and NO_y made from the aircraft. Through comparing plume ozone mixing ratios with ΣAN and the surrogate species NO_z we found that ozone production was less efficient in younger plumes aged less than 5 days with between two and eight ppbv of O_x produced per ppbv of ΣAN and between zero and two ppbv of O_x produced per ppbv of NO_x that was oxidized. In aged plumes the ozone production efficiency increased significantly to 473 ppbv O_x per ppbv ΣAN and 155 ppbv O_x per ppbv NO_z. We found that the plume ozone production efficiency was strongly correlated with the aerosol loading of the air mass with higher aerosol loading (black carbon mass concentration $> 0.1\,\mu g\,cm^{-3}$) generally associated with younger plumes and lower enhancement ratios of $\Delta O_x/\Delta NO_z$, and lower aerosol loading (black carbon mass concentration $< 0.1\,\mu g\,cm^{-3}$) in the aged plumes. When compared against NO_x, the $\Delta O_x/\Delta NO_z$ ratios indicated that the BORTAS plume measurements were made in different chemical regimes: a more VOC-limited regime for flight B626 and the high aerosol loading measurements, and a more NO_x-limited regime for the low aerosol loading measurements. Furthermore, we found that measurements of plume air with high aerosol loading and relatively low ozone production efficiency were made at high relative humidity (> 40 %) throughout the vertical extent of the troposphere and the low aerosol plumes with relatively high ozone production efficiency were made at low relative humidity and generally higher altitude (typically above 4 km).

When the BORTAS measurements were compared to similar measurements made in boreal biomass burning plumes over Eastern Canada by the ARCTAS-B and ABLE 3B campaigns we found that ozone production efficiency increased with plume ages calculated by NMHC and NO_x/NO_y ratios. In all campaign measurements we found that plumes with high aerosol loading had low ozone production efficiencies, less than 80 ppbv ppbv^{-1}. Aged plumes were typically associated with low aerosol loading and relatively high ozone production efficiency. The relatively low rate of ozone production efficiency in the plumes with high aerosol loading could be due to three possibilities: (1) increased optical depth of the plume attenuating the actinic flux and subsequent photolysis of NO_2 to form ozone; (2) potential loss of ozone and NO_y species through heterogeneous uptake by aerosol in biomass burning plumes (Longfellow et al., 2000; Grassian, 2001); and (3) light induced heterogeneous photochemical ozone loss on the surface of biomass burning aerosols that increases with relative humidity (Konovalov et al., 2012).

Other potential factors, not considered in the analysis presented here, could have influenced the tropospheric ozone distribution observed over the course of the BORTAS campaign. Many of the measurements were made downwind from potential anthropogenic emissions sources such the Northeastern US and the Alberta tar sands and while great care was taken to avoid pollution outflow from these sources in the deployment of the BORTAS aircraft campaign they could provide additional sources of VOCs and NO_x (from PAN decomposition) and influence ozone production over the BORTAS region. Measurements were also made downwind of lightning activity across North America, and could provide an additional source of NO_x in the free troposphere. Finally, ozone enhancements in boreal biomass burning plumes with low aerosol loading and low relative humidity could have been influenced by mixing of the plumes with air of stratospheric origin. Numerical models of atmospheric chemistry and transport can be used to investigate these factors, their influence on ozone production in boreal biomass burning plumes and its subsequent impact on tropospheric oxidant chemistry.

Acknowledgements. The BORTAS project is funded by the Natural Environment Research Council (NERC) under grant NE/F017391/1. Airborne data were obtained using the BAe-146-301 Atmospheric Research Aircraft (ARA) operated by Directflight Ltd (DFL) and managed by the Facility for Airborne Atmospheric Measurements (FAAM), which is a joint entity of NERC and the UK Meteorological Office. We acknowledge the great efforts provided by the staff of FAAM, DFL, Avalon Aero Ltd and Captains Alan Foster and Charlie Whittaker and First Officer Ian Ramsay-Rae. The ARCTAS-B 60-s merges were obtained from the POLARCAT/ARCTAS archive at the NASA Langley Research Center Atmospheric Science Data Center (LaRC DACC). The ABLE 3B 90-s merges were obtained from the NASA Global Tropospheric Experiment data archive at the LaRC DACC. We acknowledge Andrew Weinheimer, Armin Wisthaler, Glenn Diskin, and Yutaka Kondo for their respective measurements of $NO_x/NO_y/O_3$, CH_3CN, CO, and black carbon made during the ARCTAS-B measurement campaign as well as the science teams of ARCTAS and ABLE 3B for use of the measurements taken during each campaign.

References

Alvarado, M. J., Logan, J. A., Mao, J., Apel, E., Riemer, D., Blake, D., Cohen, R. C., Min, K.-E., Perring, A. E., Browne, E. C., Wooldridge, P. J., Diskin, G. S., Sachse, G. W., Fuelberg, H., Sessions, W. R., Harrigan, D. L., Huey, G., Liao, J., Case-Hanks, A., Jimenez, J. L., Cubison, M. J., Vay, S. A., Weinheimer, A. J., Knapp, D. J., Montzka, D. D., Flocke, F. M., Pollack, I. B., Wennberg, P. O., Kurten, A., Crounse, J., Clair, J. M. St., Wisthaler, A., Mikoviny, T., Yantosca, R. M., Carouge, C. C., and Le Sager, P.: Nitrogen oxides and PAN in plumes from boreal fires during ARCTAS-B and their impact on ozone: an integrated analysis of aircraft and satellite observations, Atmos. Chem. Phys., 10, 9739–9760, doi:10.5194/acp-10-9739-2010, 2010. 1799, 1813

Anderson, B. E., Gregory, G. L., Barrick, J. D. W., Collins Jr., J. E., Sachse, G. W., Shipham, M. C., and Hudgins, C. H.: Summertime tropospheric ozone distributions over central and eastern Canada, J. Geophys. Res., 99, 1781–1792, 1994. 1799, 1805

Anderson, T. L. and Ogren, J. A.: Determining aerosol radiative properties using the TSI 3563 integrating nephelometer, Aerosol Sci. Tech., 29, 57–69, 1998. 1804

Atkinson, R. and Arey, J.: Atmospheric degradation of volatile organic compounds, Chem. Rev., 103, 4605–4638, 2003. 1810

Atkinson, R., Baulch, D. L., Cox, R. A., Crowley, J. N., Hampson, R. F., Hynes, R. G., Jenkin, M. E., Rossi, M. J., and Troe, J.: Evaluated kinetic and photochemical data for atmospheric chemistry: Volume I – gas phase reactions of O_x, HO_x, NO_x and SO_x species, Atmos. Chem. Phys., 4, 1461–1738, doi:10.5194/acp-4-1461-2004, 2004. 1819, 1821

Bange, H. W. and Williams, J.: New directions: acetonitrile in atmospheric and biogeochemical cycles, Atmos. Environ., 34, 4959–4960, 2000. 1805

Bertschi, I. T. and Jaffe, D. A.: Long-range transport of ozone, carbon monoxide, and aerosols to the NE Pacific troposphere during the summer of 2003: observations of smoke plumes from Asian boreal fires, J. Geophys. Res., 110, D05303, doi:10.1029/2004JD005135, 2005. 1814

Blake, D. R., Smith Jr., T. W., Chen, T.-Y., Whipple, W. J., and Rowland, F. S.: Effects of biomass burning on summertime nonmethane hydrocarbon concentrations in the Canadian wetlands, J. Geophys. Res., 99, 1699–1719, 1994. 1823

Cantrell, C. A., Mauldin, L., Zondlo, M., Eisele, F., Kosiuch, E., Shetter, R., Lefer, B., Hall, S., Campos, T., Ridley, B., Walega, J., Fried, A., Wert, B., Flocke, F., Weinheimer, A., Hannigan, J., Coffey, M., Atlas, E., Stephens, S., Heikes, B., Snow, J., Blake, D., Blake, N., Katzenstein, A., Lopez, J., Browell, E. V., Dibb, J., Scheuer, E., Seid, G., and Talbot, R.: Steady state free radical budgets and ozone photochemistry during TOPSE, J. Geophys. Res., 108, 8361, doi:10.1029/2002JD002198, 2003. 1819, 1820

Cook, P. A., Savage, N. H., Turquety, S., Carver, G. D., O'Connor, F. M., Heckel, A., Stewart, D., Whalley, L. K., Parker, A. E., Schlager, H., Singh, H. B., Avery, M. A., Sachse, G. W., Brune, W., Richter, A., Burrows, J. P., Purvis, R., Lewis, A. C., Reeves, C. E., Monks, P. S., Levine, J. G., and Pyle, J. A.: Forest fire plumes over the North Atlantic: p-TOMCAT model simulations with aircraft and satellite measurements from the ITOP/ICARTT campaign, J. Geophys. Res., 112, D10S43, doi:10.1029/2006JD007563, 2007. 1800

Dari-Salisburgo, C., Di Carlo, P., Giammaria, F., Kajii, Y., and D'Altorio, A.: Laser induced fluorescence instrument for NO_2 measurements: observations at a central Italy background site, Atmos. Environ., 43, 970–977, 2009. 1804

Day, D. A., Dillon, M. B., Wooldridge, P. J., Thornton, J. A., Rosen, R. S., Wood, E. C., and Cohen, R. C.: On alkyl nitrates, O_3, and the "missing NO_y", J. Geophys. Res., 108, 4501, doi:10.1029/2003JD003685, 2003. 1803

DeBell, L. J., Talbot, R. W., Dibb, J. E., Munger, J. W., Fischer, E. V., and Frolking, S. E.: A major regional air pollution event in the northeastern United States caused by extensive forest fires in Quebec, Canada, J. Geophys. Res., 109, D19305, doi:10.1029/2004JD004840, 2004. 1813

Di Carlo, P., Aruffo, E., Busilacchio, M., Giammaria, F., Dari-Salisburgo, C., Biancofiore, F., Visconti, G., Lee, J., Moller, S., Reeves, C. E., Bauguitte, S., Forster, G., Jones, R. L., and Ouyang, B.: Aircraft based four-channel thermal dissociation laser induced fluorescence instrument for simultaneous measurements of NO_2, total peroxy nitrate, total alkyl nitrate, and HNO_3, Atmos. Meas. Tech. Discuss., 5, 8759–8787, doi:10.5194/amtd-5-8759-2012, 2012. 1804

Fehsenfeld, F. C., Ancellet, G., Bates, T. S., Goldstein, A. H., Hardesty, R. M., Honrath, R., Law, K. S., Lewis, A. C., Leaitch, R., McKeen, S., Meagher, J., Parrish, D. D., Pszenny, A. A. P., Russell, P. B., Schlager, H., Seinfeld, J., Talbot, R., and Zbinden, R.: International consortium for atmospheric research on transport and transformation (ICARTT): north America to Europe – overview of the 2004 summer field study, J. Geophys. Res., 111, D23S01, doi:10.1029/2006JD007829, 2006. 1799

Gerbig, C., Schmitgen, S., Kley, D., and Volz-Thomas, A.: An improved fast-response vacuum-UV resonance fluorescence CO instrument, J. Geophys. Res., 104, 1699–1704, 1999. 1803

Goode, J. G., Yokelson, R. J., Ward, D. E., Susott, R. A., Babbitt, R. E., Davies, M. A., and Hao, W. M.: Measurements of excess O_3, CO_2, CO, CH_4, C_2H_4, C_2H_2, HCN, NO, NH_3, HCOOH, CH_3COOH, HCHO, and CH_3OH in 1997 Alaskan biomass burning plumes by airborne Fourier transform infrared spectroscopy (AFTIR), J. Geophys. Res., 105, 22147–22166, 2000. 1813

Grassian, V. H.: Heterogeneous uptake and reaction of nitrogen oxides and volatile organic compounds on the surface of atmospheric particles including oxides, carbonates, soot and mineral dust: implications for the chemical balance of the troposphere, Int. Rev. Phys. Chem., 20, 467–548, 2001. 1826

Griffin, R. J., Beckman, P. J., Talbot, R. W., Sive, B. C., and Varner, R. K.: Deviations from ozone photostationary state during the international consortium for atmospheric research on transport and transformation 2004 campaign: use of measurements and photochemical modeling to assess potential causes, J. Geophys. Res., 112, D10S07, doi:10.1029/2006JD007604, 2007. 1819, 1820, 1821

Harriss, R. C., Wofsy, S. C., Bartlett, D. S., Shipham, M. C., Jacob, D. J., Hoell Jr., J. M., Bendura, R. J., Drewry, J. W., McNeal, R. J., Navarro, R. L., Gidge, R. N., and Rabine, V. E.: The arctic boundary layer expedition (ABLE 3A): July–August 1988, J. Geophys. Res., 97, 16383–16394, 1992. 1799

Harriss, R. C., Wofsy, S. C., Hoell Jr., J. M., Bendura, R. J., Drewry, J. W., McNeal, R. J., Pierce, D., Rabine, V., and Snell, R. L.: The arctic boundary layer expedition (ABLE 3B): July–August 1990, J. Geophys. Res., 99, 1635–1643, 1994. 1799, 1821, 1823

Helmig, D., Tanner, D. M., Honrath, R. E., Owen, R. C., and Parrish, D. D.: Nonmethane hydrocarbons at Pico Mountain, Azores: 1. oxidation chemistry in the North Atlantic region, J. Geophys. Res., 113, D20S91, doi:10.1029/2007JD008930, 2008. 1799, 1810

Honrath, R. E., Owen, R. C., Val Martin, M., Reid, J. S., Lapina, K., Fialho, P., Dziobak, M. P., Kleissl, J., and Westphal, D. L.: Regional and hemispheric impacts of anthropogenic and biomass burning emissions on summertime CO and O_3 in the North Atlantic lower free troposphere, J. Geophys. Res., 109, D24310, doi:10.1029/2004JD005147, 2004. 1814

Hopkins, J. R., Lewis, A. C., and Read, K. A.: A two-column method for long-term monitoring of non-methane hydrocarbons (NMHCs) and oxygenated volatile organic compounds (o-VOCs), J. Environ. Monitor., 5, 8–13, 2003. 1804

Hopkins, J. R., Jones, C. E., and Lewis, A. C.: A dual channel gas chromatograph for atmospheric analysis of volatile organic compounds including oxygenated and monoterpene compounds, J. Environ. Monitor., 13, 2268–2276, 2011. 1804

Jacob, D. J., Crawford, J. H., Maring, H., Clarke, A. D., Dibb, J. E., Emmons, L. K., Ferrare, R. A., Hostetler, C. A., Russell, P. B., Singh, H. B., Thompson, A. M., Shaw, G. E., McCauley, E., Pederson, J. R., and Fisher, J. A.: The Arctic Research of the Composition of the Troposphere from Aircraft and Satellites (ARCTAS) mission: design, execution, and first results, Atmos. Chem. Phys., 10, 5191–5212, doi:10.5194/acp-10-5191-2010, 2010. 1821

Jaffe, D. A. and Wigder, N. L.: Ozone production from wildfires: a critical review, Atmos. Environ., 51, 1–10, 2012. 1800, 1813, 1814, 1825, 1839

Jobson, B. T., Wu, Z., Niki, H., and Barrie, L. A.: Seasonal trends of isoprene, C_2–C_5 alkanes, and acetylene at a remote boreal site in Canada, J. Geophys. Res., 99, 1589–1599, 1994. 1810

Kleinman, L. I.: Ozone process insights from field experiments – Part II: Observation-based analysis for ozone production, Atmos. Environ., 34, 2023–2033, 2000. 1803

Kondo, Y., Matsui, H., Moteki, N., Sahu, L., Takegawa, N., Kajino, M., Zhao, Y., Cubison, M. J., Jimenez, J. L., Vay, S., Diskin, G. S., Anderson, B., Wisthaler, A., Mikoviny, T., Fuelberg, H. E., Blake, D. R., Huey, G., Weinheimer, A. J., Knapp, D. J., and Brune, W. H.: Emissions of black carbon, organic, and inorganic aerosols from biomass burning in North America and Asia in 2008, J. Geophys. Res., 116, D08204, doi:10.1029/2010JD015152, 2011. 1822

Konovalov, I. B., Beekman, M., D'Anna, B., and George, C.: Significant light induced ozone loss on biomass burning aerosol: evidence from chemistry-transport modeling based on new laboratory studies, Geophys. Res. Lett., 39, L17807, doi:10.1029/2012GL052432, 2012. 1826

Laborde, M., Mertes, P., Zieger, P., Dommen, J., Baltensperger, U., and Gysel, M.: Sensitivity of the Single Particle Soot Photometer to different black carbon types, Atmos. Meas. Tech., 5, 1031–1043, doi:10.5194/amt-5-1031-2012, 2012. 1804

Lapina, K., Honrath, R. E., Owen, R. C., Val Martin, M., and Pfister, G.: Evidence of significant large-scale impacts of boreal fires on ozone levels in the midlatitude Northern Hemisphere free troposphere, Geophys. Res. Lett., 33, L10815, doi:10.1029/2006GL025878, 2006. 1799

Lee, J. D., Moller, S. J., Read, K. A., Lewis, A. C., Mendes, L., and Carpenter, L. J.: Year-round measurements of nitrogen oxides and ozone in the tropical North Atlantic marine boundery layer, J. Geophys. Res., 114, D21302, doi:10.1029/2009JD011878, 2009. 1804

Leighton, P. A.: Photochemistry of Air Pollution, Elsevier, New York, 1961. 1819

Lewis, A. C., Evans, M. J., Methven, J., Watson, N., Lee, J. D., Hopkins, J. R., Purvis, R. M., Arnold, S. R., McQuaid, J. B., Whalley, L. K., Pilling, M. J., Heard, D. E., Monks, P. S., Parker, A. E., Reeves, C. E., Oram, D. E., Mills, G., Bandy, B. J., Stewart, D., Coe, H., Williams, P., and Crosier, J.: Chemical composition observed over the mid-Atlantic and the detection of pollution signatures far from source regions, J. Geophys. Res., 112, D10S39, doi:10.1029/2006JD007584, 2007. 1799

Longfellow, C. A., Ravishankara, A. R., and Hanson, D. R.: Reactive and nonreactive uptake on hydrocarbon soot: HNO_3, O_3, and N_2O_5, J. Geophys. Res., 105, 24345–24350, 2000. 1826

Mauzerall, D. L., Jacob, D. J., Fan, S.-M., Bradshaw, J. D., Gregory, G. L., Sachse, G. W., and Blake, D. R.: Origin of tropospheric ozone at remote high northern latitudes in summer, J. Geophys. Res., 101, 4175–4188, 1996. 1800, 1813

McKeen, S. A., Wotawa, G., Parrish, D. D., Holloway, J. S., Buhr, M. P., Hübler, G., Fehsenfeld, F. C., and Meagher, J. F.: Ozone production from Canadian wildfires during June and July of 1995, J. Geophys. Res., 107, 4192, doi:10.1029/2001JD000697, 2002. 1800

McMeeking, G. R., Hamburger, T., Liu, D., Flynn, M., Morgan, W. T., Northway, M., Highwood, E. J., Krejci, R., Allan, J. D., Minikin, A., and Coe, H.: Black carbon measurements in the boundary layer over western and northern Europe, Atmos. Chem. Phys., 10, 9393–9414, doi:10.5194/acp-10-9393-2010, 2010. 1804

Moteki, N. and Kondo, Y.: Effects of mixing state on black carbon measurements by laser-induced incandescence, Aerosol Sci. Tech., 41, 398–417, 2007. 1822

Murphy, J. G., Oram, D. E., and Reeves, C. E.: Measurements of volatile organic compounds over West Africa, Atmos. Chem. Phys., 10, 5281–5294, doi:10.5194/acp-10-5281-2010, 2010. 1803

Olszyna, K. J., Bailey, E. M., Simonaitis, R., and Meagher, J. F.: O_3 and NO_y relationships at a rural site, J. Geophys. Res., 99, 14557–14563, 1994. 1803, 1820

Palmer, P. I., Parrington, M., Lee, J. D., Lewis, A. C., Rickard, A. R., Bernath, P. F., Duck, T. J., Waugh, D. L., Tarasick, D. W., Andrews, S., Aruffo, E., Bailey, L., Barratt, E. M., Bauguitte, S. J.-B., Curry, K. R., Di Carlo, P., Chisholm, L., Dan, L., Forster, G., Franklin, J. E., Gibson, M., Griffin, D., Helmig, D., Hopkins, J. R., Hopper, J. T., Jenkin, M. E., Kindred, D., Kliever, J., Le Breton, M., Matthiesen, S., Maurice, M., Moller, S. J., Moore, D. P., Oram, D. E., O'Shea, S. J., Owen, R. C., Pagniello, C. M. L. S., Percival, C. J., Pierce, J. R., Punjabi, S., Remedios, J. J., Rotermund, K. J., Sakamoto, K. M., Strawbridge, K. B., Strong, K., Taylor, J. W., Trigwell, R., Tereszchuk, K. A., Walker, K. A., Weaver, D., Whaley, C., and Young, J. C.: Quantifying the impact of BOReal forest fires on Tropospheric oxidants over the Atlantic using Arcraft and Satellites (BORTAS) experiment: design, execution and first results, Atmos. Chem. Phys. Discuss., submitted, 2012. 1798, 1803, 1805

Parrington, M., Palmer, P. I., Henze, D. K., Tarasick, D. W., Hyer, E. J., Owen, R. C., Helmig, D., Clerbaux, C., Bowman, K. W., Deeter, M. N., Barratt, E. M., Coheur, P.-F., Hurtmans, D., Jiang, Z., George, M., and Worden, J. R.: The influence of boreal biomass burning emissions on the distribution of tropospheric ozone over North America and the North Atlantic during 2010, Atmos. Chem. Phys., 12, 2077–2098, doi:10.5194/acp-12-2077-2012, 2012. 1798

Parrish, D. D., Hahn, C. J., Williams, E. J., Norton, R. B., Fehsenfeld, F. C., Singh, H. B., Shetter, J. D., Gandrud, B. W., and Ridley, B. A.: Indications of photochemical histories of Pacific air masses from measurements of atmospheric trace species at Point Arena, California, J. Geophys. Res., 97, 15883–15901, 1992. 1810

Parrish, D. D., Holloway, J. S., Trainer, M., Murphy, P. C., Forbes, G. L., and Fehsenfeld, F. C.: Export of North American ozone pollution to the North Atlantic ocean, Science, 259, 1436–1439, 1993. 1812

Parrish, D. D., Stohl, A., Forster, C., Atlas, E. L., Blake, D. R., Goldan, P. D., Kuster, W. C., and de Gouw, J. A.: Effects of mixing on evolution of hydrocarbon ratios in the troposphere, J. Geophys. Res., 112, D10S34, doi:10.1029/2006JD007583, 2007. 1809, 1810, 1825

Perring, A. E., Bertram, T. H., Farmer, D. K., Wooldridge, P. J., Dibb, J., Blake, N. J., Blake, D. R., Singh, H. B., Fuelberg, H., Diskin, G., Sachse, G., and Cohen, R. C.: The production and persistence of $\Sigma RONO_2$ in the Mexico City plume, Atmos. Chem. Phys., 10, 7215–7229, doi:10.5194/acp-10-7215-2010, 2010. 1802, 1816

Pfister, G. G., Emmons, L. K., Hess, P. G., Honrath, R., Lamarque, J.-F., Val Martin, M., Owen, R. C., Avery, M. A., Browell, E. V., Holloway, J. S., Nedelec, P., Purvis, R., Ryerson, T. B., Sachse, G. W., and Schlager, H.: Ozone production from the 2004 North American boreal fires, J. Geophys. Res., 111, D24S07, doi:10.1029/2006JD007695, 2006. 1800, 1812, 1814

Real, E., Law, K. S., Weinzierl, B., Fiebig, M., Petzold, A., Wild, O., Methven, J., Arnold, S., Stohl, A., Huntrieser, H., Roiger, A., Schlager, H., Stewart, D., Avery, M., Sachse, G., Browell, E., Ferrare, R., and Blake, D.: Processes influencing ozone levels in Alaskan forest fire plumes during long-range transport over the North Atlantic, J. Geophys. Res., 112, D10S41, doi:10.1029/2006JD007576, 2007. 1800

Rickard, A. R., Salisbury, G., Monks, P. S., Lewis, A. C., Baugitte, S., Bandy, B. J., Clemitshaw, K. C., and Penkett, S. A.: Comparison of measured ozone production efficiencies in the marine boundary layer at two European coastal sites under different pollution regimes, J. Atmos. Chem., 43, 107–134, 2002. 1803, 1817

Rudolph, J. and Johnen, F. J.: Measurements of light atmospheric hydrocarbons over the Atlantic in regions of low biological activity, J. Geophys. Res., 95, 20583–20591, 1990. 1810

Sachse, G. W., Hill, G. F., Wade, L. O., and Perry, M. G.: Fast-response, high-precision carbon monoxide sensor using a tunable diode laser absorption technique, J. Geophys. Res., 92, 2071–2081, 1987. 1822

Sandholm, S., Olson, J., Bradshaw, J., Talbot, R., Singh, H., Gregory, G., Blake, D., Anderson, B., Sachse, G., Barrick, J., Collins, J., Klemm, K., Lefer, B., Klemm, O., Gorzelska, K., Herlth, D., and O'Hara, D.: Summertime partitioning and budget of NO_y compounds in the troposphere over Alaske and Canada: ABLE 3B, J. Geophys. Res., 99, 1837–1861, 1994. 1823

Schwarz, J. P., Gao, R. S., Fahey, D. W., Thomson, D. S., Watts, L. A., Wilson, J. C., Reeves, J. M., Darbehesti, M., Baumgardner, D. G., Kok, G. L., Chung, S. H., Schulz, M., Hendricks, J., Lauer, A., Kärcher, B., Slowik, J. G., Rosenlof, K. H., Thompson, T. L., Langford, A. O., Loewenstein, M., and Aikin, K. C.: Single-particle measurements of midlatitude black carbon and light-scattering aerosols from the boundary layer to the lower stratosphere, J. Geophys. Res., 111, D16207, doi:10.1029/2006JD007076, 2006. 1804

Singh, H. B., Anderson, B. E., Brune, W. H., Cai, C., Cohen, R. C., Crawford, J. H., Cubison, M. J., Czech, E. P., Emmons, L., Fuelberg, H. E., Huey, G., Jacob, D. J., Jimenez, J. L., Kaduwela, A., Kondo, Y., Mao, J., Olson, J. R., Sachse, G. W., Vay, S. A., Weinheimer, A., Wennberg, P. O., Wisthaler, A., and the ARCTAS Science Team: Pollution influences on atmospheric composition and chemistry at high northern latitudes: boreal and California forest fire emissions, Atmos. Environ., 44, 4553–4564, 2010. 1799, 1813

Spivakovsky, C. M., Logan, J. A., Montzka, S. A., Balkanski, Y. J., Foreman-Fowler, M., Jones, D. B. A., Horowitz, L. W., Fusco, A. C., Brenninkmeijer, C. A. M., Prather, M. J., Wofsy, S. C., and McElroy, M. B.: Three-dimensional climatological distribution of tropospheric OH: update and evaluation, J. Geophys. Res., 105, 8931–8980, 2000. 1810

Tanimoto, H., Matsumoto, K., and Uematsu, M.: Ozone-CO correlations in Siberian wildfire plumes observed at Rishiri Island, SOLA, 4, 65–68, doi:10.2151/sola.2008-017, 2008. 1813

Trainer, M., Parrish, D. D., Buhr, M. P., Norton, R. B., Fehsenfeld, F. C., Anlauf, K. G., Bottenheim, J. W., Tang, Y. Z., Wiebe, H. A., Roberts, J. M., Tanner, R. L., Newman, L., Bowersox, V. C., Meagher, J. F., Olszyna, K. J., Rodgers, M. O., Wang, T., Berresheim, H., Demerjian, K. L., and Roychowdhury, U. K.: Correlation of ozone with NO_y in photochemically aged air, J. Geophys. Res., 98, 2917–2925, 1993. 1803

Val Martin, M., Honrath, R. E., Owen, R. C., Pfister, G., Fialho, P., and Barata, F.: Significant enhancements of nitrogen oxides, black carbon, and ozone in the North Atlantic lower free troposphere resulting from North American boreal wildfires, J. Geophys. Res., 111, D23S60, doi:10.1029/2006JD007530, 2006. 1799, 1814

Volz-Thomas, A., Lerner, A., Pätz, H.-W., Schulz, M., McKenna, D. S., Schmitt, S., Madronich, S., and Röth, E. P.: Airborne measurements of the photolysis frequency of NO_2, J. Geophys. Res., 101, 18613–18627, 1996. 1804

Wang, T., Carroll, M. A., Albercook, G. M., Owens, K. R., Duderstadt, K. A., Markevitch, A. N., Parrish, D. D., Holloway, J. S., Fehsenfeld, F. C., Forbes, G., and Ogren, J.: Ground-based measurements of NO_x and total reactive oxidized nitrogen (NO_y) at Sable Island, Nova Scotia, during the NARE 1993 summer intensive, J. Geophys. Res., 101, 28991–29004, 1996. 1817

Weinheimer, A. J., Walega, J. G., Ridley, B. A., Gary, B. L., Blake, D. R., Blake, N. J., Rowland, F. S., Sachse, G. W., Anderson, B. E., and Collins, J. E.: Meridional distributions of NO_x, NO_y, and other species in the lower stratosphere and upper troposphere during AASE II, Geophys. Res. Lett., 21, 2583–2586, 1994. 1822

Wilson, K. L. and Birks, J. W.: Mechanism and elimination of a water vapor interference in the measurement of ozone by UV absorbance, Environ. Sci. Technol., 40, 6361–6367, 2006. 1803

Wisthaler, A., Hansel, A., Dickerson, R. R., and Crutzen, P. J.: Organic trace gas measurements by PTR-MS during INDOEX 1999, J. Geophys. Res., 107, 8024, doi:10.1029/2001JD000576, 2002. 1822

Wofsy, S. C., Sachse, G. W., Gregory, G. L., Blake, D. R., Bradshaw, J. D., Sandholm, S. T., Singh, H. B., Barrick, J. A., Harriss, R. C., Talbot, R. W., Shipham, M. A., Browell, E. V., Jacob, D. J., and Logan, J. A.: Atmospheric chemistry in the Arctic and Subarctic: influence of natural fires, industrial emissions, and stratospheric inputs, J. Geophys. Res., 97, 16731–16746, 1992. 1799

Title Page
Abstract | Introduction
Conclusions | References
Tables | Figures
◀| |▶
◀ ▶
Back | Close
Full Screen / Esc
Printer-friendly Version
Interactive Discussion

Wofsy, S. C., Fan, S.-M., Blake, D. R., Bradshaw, J. D., Sandholm, S. T., Singh, H. B., Sachse, G. W., and Harriss, R. C.: Factors influencing atmospheric composition over subarctic North America during summer, J. Geophys. Res., 99, 1887–1897, 1994. 1823

Table 1. Flight IDs, dates, and location of research flights made by the BAe-146 during the BORTAS aircraft measurement campaign in 2011.

Flight ID	Date (Day of Year)	Location
B620	15 Jul (196)	Eastern Quebec
B621	18 Jul (199)	Newfoundland and Labrador
B622	20 Jul (201)	Southern Quebec
B623	20 Jul (201)	Quebec City to Halifax
B624	21 Jul (202)	Atlantic Ocean to east of Island of Newfoundland
B625	24 Jul (202)	Gulf of St. Lawrence
B626	26 Jul (207)	Northwestern Ontario
B627	27 Jul (208)	Thunder Bay ON to Goose Bay NL
B628	28 Jul (209)	Labrador coast
B629	31 Jul (212)	Gulf of St. Lawrence
B630	31 Jul (212)	Nova Scotia and Island of Newfoundland

Table 2. Statistics for measured ozone distributions on each research flight during the BORTAS measurement campaign.

Flight ID	Mean (ppbv)	Median (ppbv)	Std. Dev. (ppbv)	Range (ppbv)
B620	50.0	47.6	12.7	28.7–105.2
B621	54.8	51.1	16.5	17.4–106.2
B621a	**66.8**	**64.9**	**18.0**	**17.4–106.2**
B621b	**47.3**	**45.8**	**9.6**	**25.9–78.4**
B622	48.2	47.5	7.7	24.4–72.9
B623	47.8	47.1	6.3	27.9–76.7
B624	54.8	54.3	7.5	31.0–84.8
B624a	**53.5**	**53.1**	**7.6**	**31.0–84.8**
B624b	**58.8**	**58.7**	**5.5**	**40.8–72.0**
B625	39.4	29.9	16.5	21.1–124.8
B626	38.7	31.3	16.0	21.5–101.4
B626a	**50.1**	**46.9**	**17.3**	**21.5–101.4**
B626b	**31.3**	**26.8**	**9.4**	**22.3–58.8**
B627	52.0	51.0	9.8	21.9–92.9
B628	49.0	47.2	15.2	24.5–119.1
B628a	**49.7**	**47.2**	**16.5**	**26.2–119.1**
B628b	**47.2**	**47.0**	**10.6**	**24.5–73.6**
B629	59.1	60.8	12.7	18.1–88.5
B630	59.6	58.8	13.1	19.8–104.1

Table 3. Observed $\Delta O_3/\Delta CO$ in biomass burning plumes sampled during BORTAS filtered by photochemical age following Jaffe and Wigder (2012).

Plume category	Range of $\Delta O_3/\Delta CO$ (ppbv ppbv^{-1}) (no. of measurements)	Mean (ppbv ppbv^{-1})	Median (ppbv ppbv^{-1})	Standard deviation (ppbv ppbv^{-1})
≤2 days[a]	0.010–0.028 ($n = 8$)	0.020	0.027	0.008
2–5 days[b]	0.02–0.42 ($n = 100$)	0.12	0.11	0.07
2–5 days (all)[c]	0.02–1.20 ($n = 134$)	0.21	0.14	0.21
≥5 days (all)[c]	0.20–3.00 ($n = 57$)	0.63	0.48	0.52
≥5 days (all)[d]	0.20–1.38 ($n = 55$)	0.55	0.47	0.29

[a] Flight B626.

[b] $[CH_3CN] > 300$ pptv.

[c] $[CH_3CN] > 150$ pptv.

[d] $\Delta O_3/\Delta CO < 2$ ppbv ppbv^{-1}.

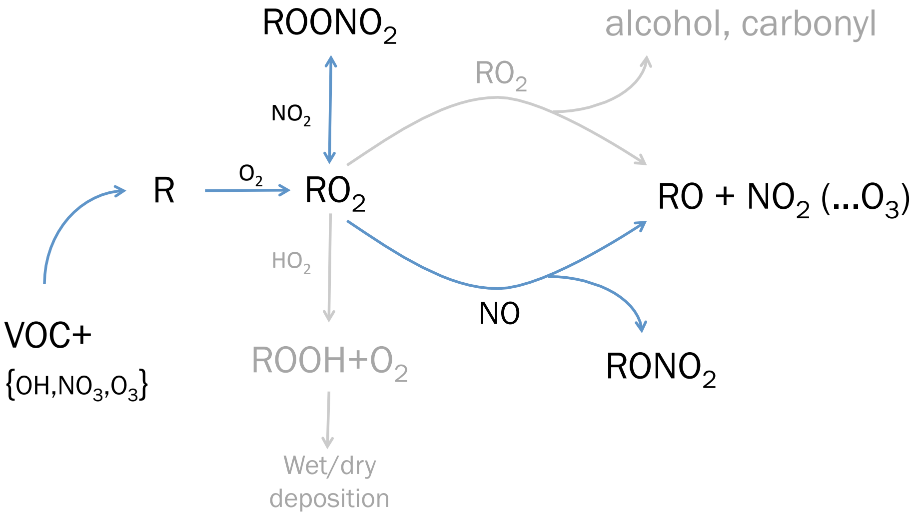

Fig. 1. Schematic of the atmospheric ozone-NO$_x$-hydrocarbon chemistry cycle studied by BORTAS.

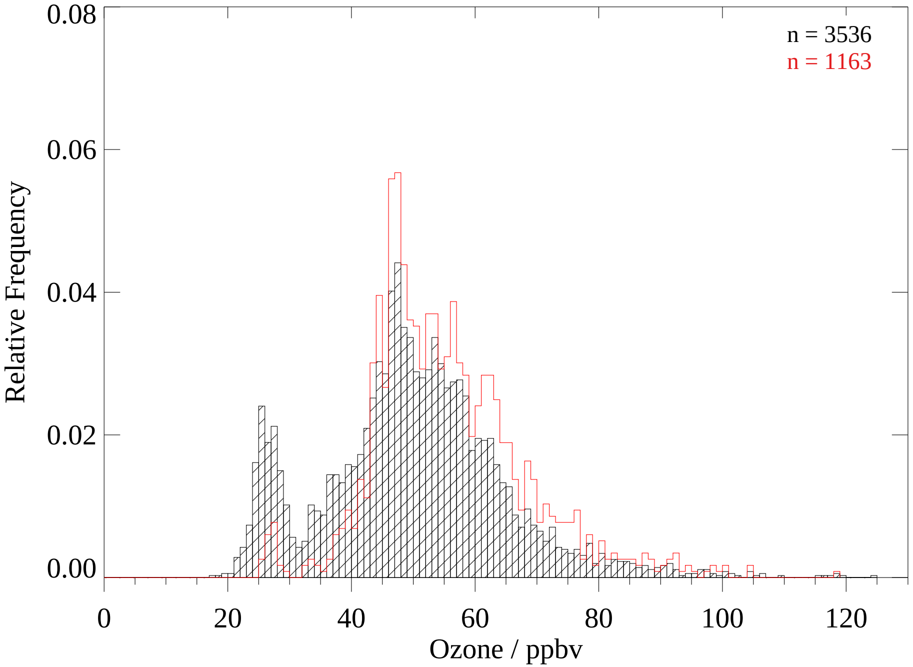

Fig. 2. Frequency distribution of ozone mixing ratios measured from the BAe-146 on all research flights during the BORTAS campaign period (15 to 31 July 2011). Frequencies are calculated for 1 ppbv bins. The black shaded area shows the distribution of all the measured ozone mixing ratios with the red line showing the distribution of measurements identified as biomass burning plumes using a threshold 150 pptv acetonitrile.

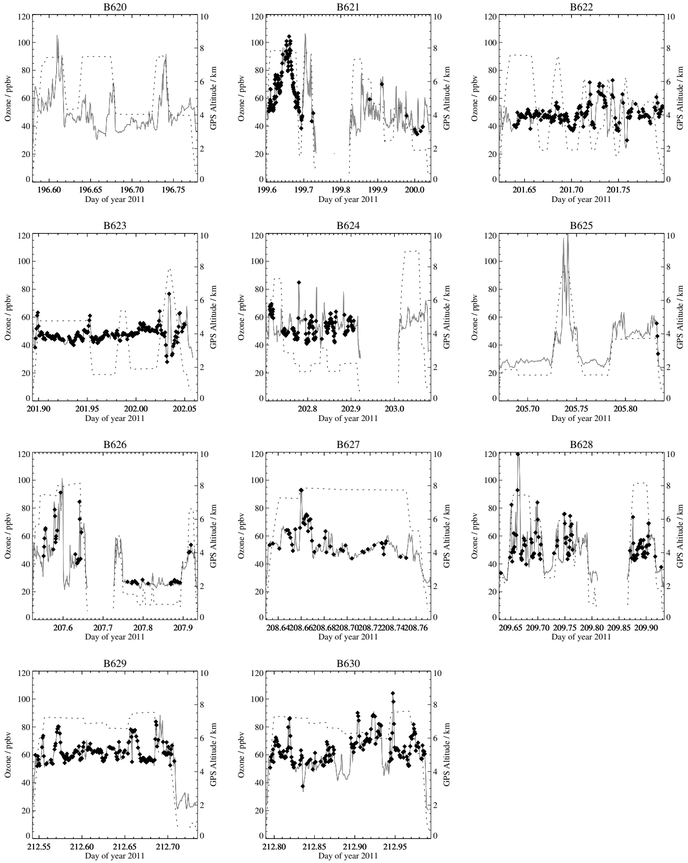

Fig. 3. Timeseries of ozone mixing ratios in ppbv measured on each research flights with the BAe-146 during the BORTAS campaign period. Grey solid lines show the 60-s average ozone mixing ratio timeseries and black diamonds show the measured ozone mixing ratio in the air masses identified as biomass burning plumes. Black dotted lines show the aircraft GPS altitude in km. Individual plot titles refer to the flight IDs listed in Table 1.

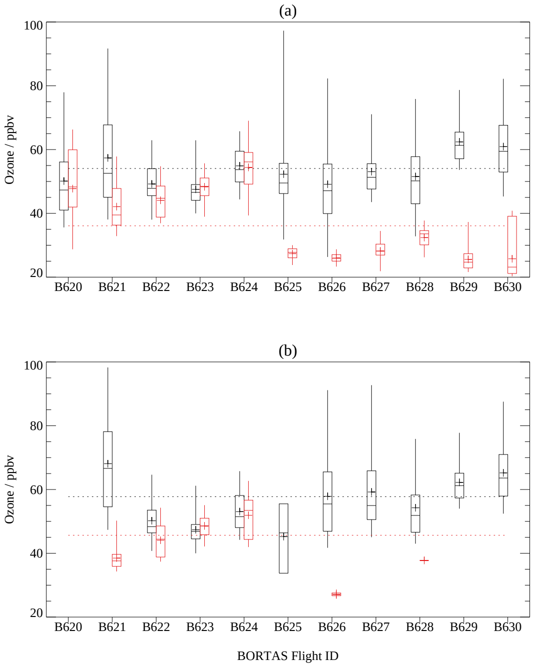

Fig. 4. Box and whisker plot of the distribution of ozone mixing ratios measured on each flight of the BORTAS measurement campaign for **(a)** all measured values, and **(b)** measurements identified as biomass burning plumes. Black boxes show data measured in the free troposphere above 3 km and red boxes show data measured in the PBL between the surface and 3 km. Dotted horizontal lines show the mean ozone mixing ratio for the ensemble of the flights shown. In each box, the central horizontal line shows the median value and the bounding horizontal lines are the upper and lower quartiles, whiskers show the range of the data between the 5th and 95th percentiles. Plus symbols show the mean value for each flight.

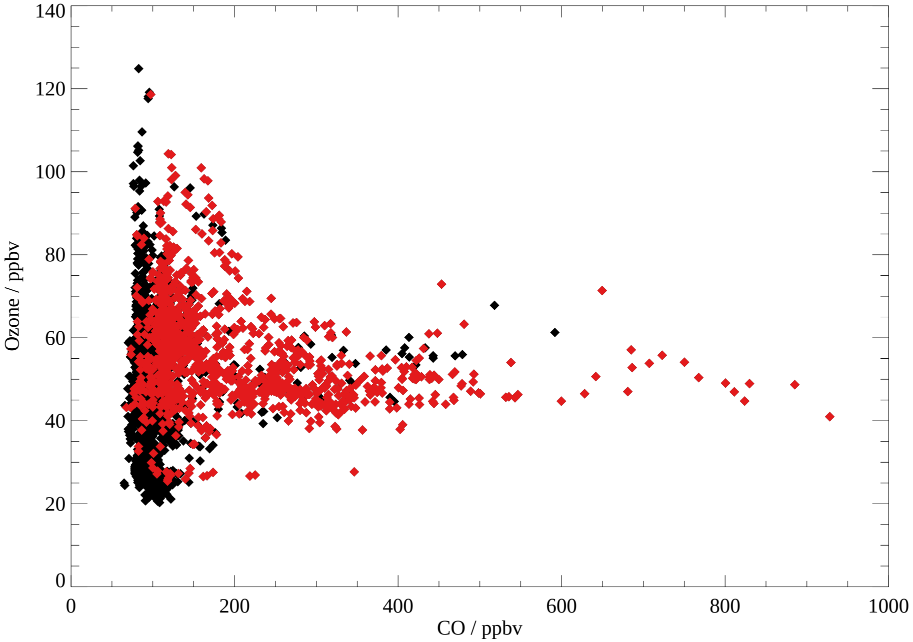

Fig. 5. Scatter plot of 60-s averaged ozone versus CO mixing ratios in ppbv measured from the BAe-146 over the BORTAS campaign period. Black symbols show all measured data and red symbols show the data points identified as biomass burning outflow.

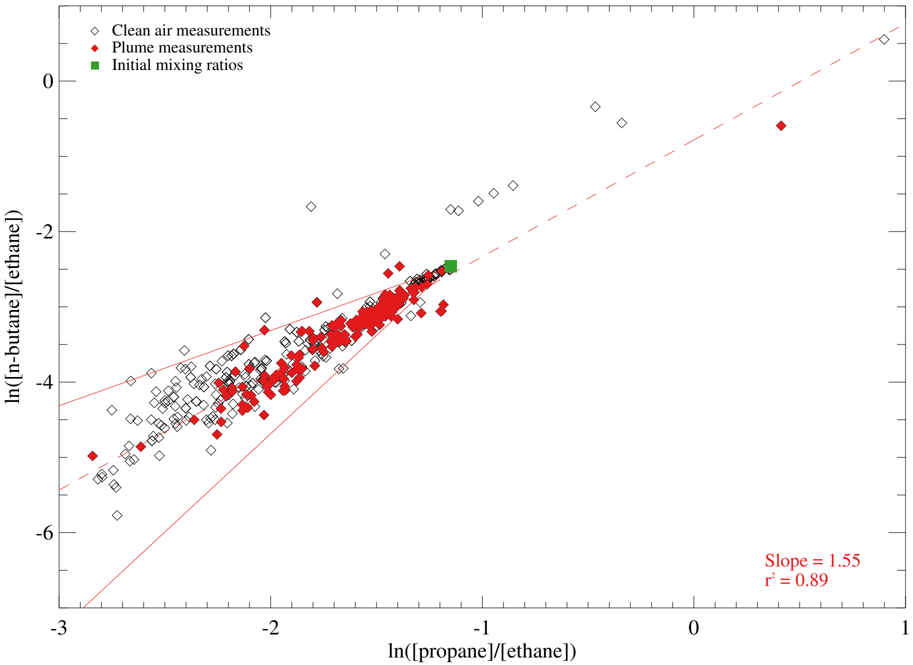

Fig. 6. Scatter plot of the natural logarithms of the ratios of *n*-butane : ethane and propane : ethane measured from whole air canister samples taken by the BAe-146 during the BORTAS campaign period. All measured data are shown as black open diamonds with red closed diamonds showing measurements made in boreal biomass burning plumes. The green square shows the ratios of the initial concentrations of the three alkanes used in the plot estimated from BORTAS flight B626 over the burning source region in Northwestern Ontario. The solid red bounding lines represent the behaviour of the hydrocarbon ratios: the steeper slope assumes only oxidation of the alkanes with OH (kinetic slope); the shallower slope assumes only mixing of fresh emissions with background air (mixing slope). The dashed red line shows a linear fit to the plume measurements.

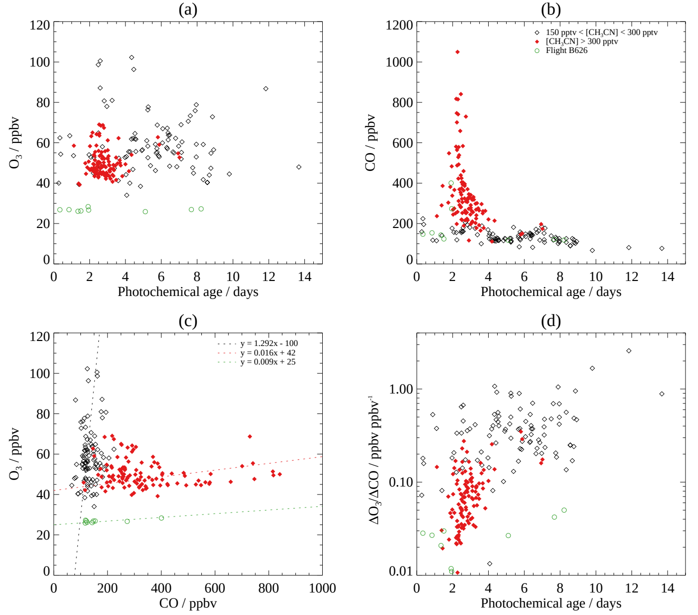

Fig. 7. Relationship between ozone and CO mixing ratios measured from the BAe-146 and sampled at the WAS measurement times, and photochemical ages calculated from the ln(propane/ethane) ratio in boreal biomass burning plumes throughout the BORTAS-B measurement campaign. Plots **(a)** and **(b)** show the measured ozone and CO mixing ratios, respectively, in units of ppbv as a function of the calculated photochemical age in days. Plot **(c)** shows the scatter of ozone versus CO with linear fitting to each population of data points shown as dotted lines. Plot **(d)** shows the enhancement of ozone relative to CO ($\Delta O_3/\Delta CO$) as a function of photochemical age. In all plots the data are filtered according to their relative abundance of acetonitrile (CH_3CN) with black open diamonds representing CH_3CN mixing ratios between 150 and 300 pptv and red closed diamonds representing CH_3CN mixing ratios in excess of 300 pptv. Measurements made on flight B626 over the fire region in Northwestern Ontario are treated separately and are represented by green open circles.

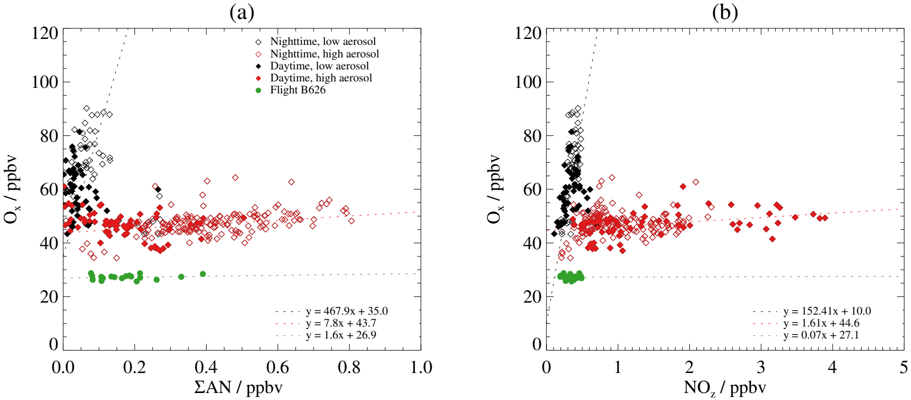

Fig. 8. Relationship between **(a)** O_x ($O_3 + NO_2$) and alkyl nitrates (ΣAN), and **(b)** O_x and NO_z (NO_y–NO_x) measured in boreal biomass burning plumes from the BAe-146 over the course of the BORTAS measurement campaign. Nighttime and daytime measurements are represented by open and closed diamonds, respectively. Black symbols represent measurement with black carbon mass concentrations less than 0.1 $\mu g\,cm^{-3}$ and red symbols with black carbon mass concentrations greater than 0.1 $\mu g\,cm^{-3}$. Measurements made on flight B626 over the fire region in Northwestern Ontario are treated separately and are represented by green circles.

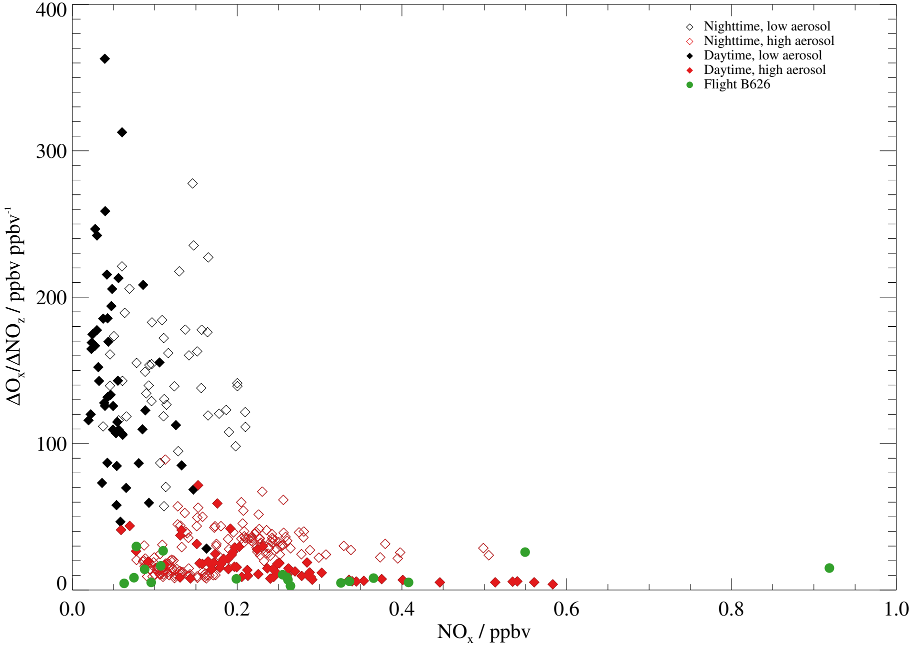

Fig. 9. Relationship between the enhancement ratio of O_x to NO_z ($\Delta O_x/\Delta NO_z$) in units of ppbv ppbv^{-1} and NO_x mixing ratio in units of ppbv measured in boreal biomass burning plumes from the BAe-146 over the course of the BORTAS measurement campaign. Symbols are the same as those described for Fig. 8.

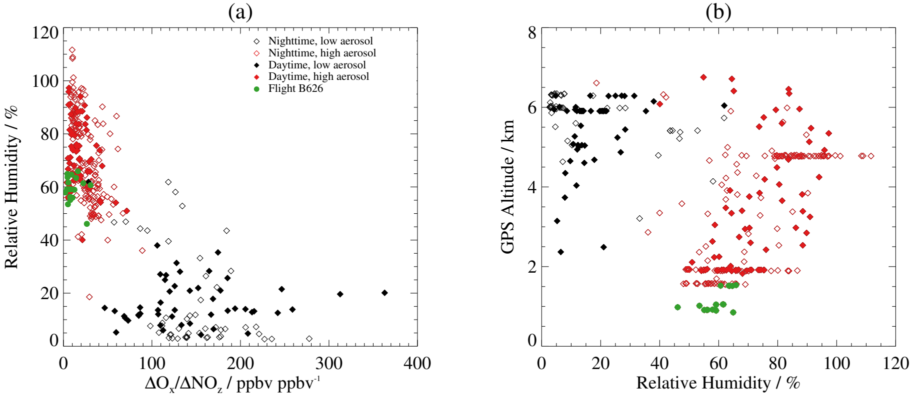

Fig. 10. Relationship between **(a)** relative humidity in percent and the ratio of the $\Delta O_x/\Delta NO_z$ ratio in units of ppbv ppbv^{-1}, and **(b)** relative humidity and aircraft GPS altitude in km measured in boreal biomass burning plumes over the course of the BORTAS measurement campaign. Symbols are the same as those described for Fig. 8.

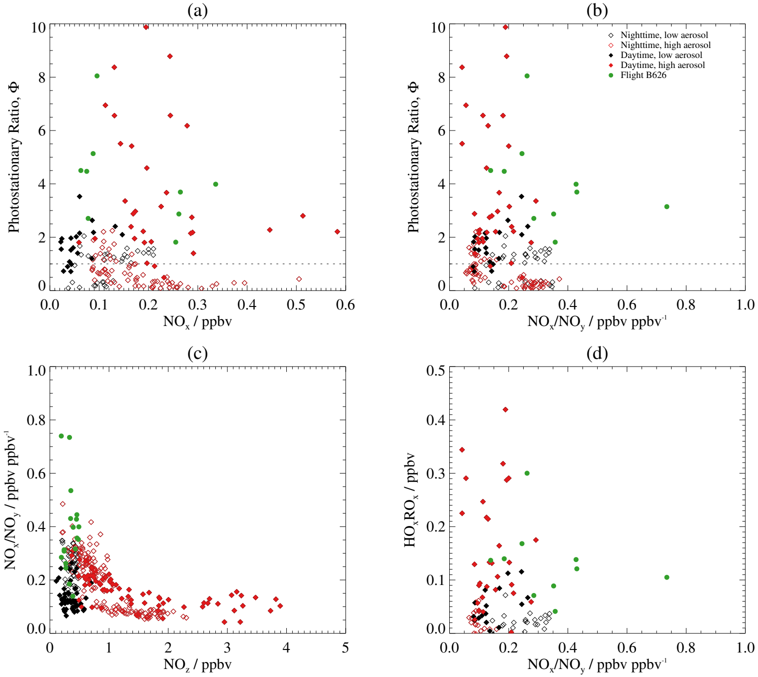

Fig. 11. Relationship between ozone photostationary state and the NO_y budget measured in boreal biomass burning plumes over the course of the BORTAS campaign. Plots **(a)** and **(b)** show the calculated photostationary ratio, Φ, versus NO_x mixing ratios (ppbv) and the ratio of NO_x to NO_y respectively. Plot **(c)** shows the relationship between NO_x/NO_y and NO_z. Plot **(d)** shows calculated total peroxy radical mixing ratios, HO_xRO_x, required for a photostationary ratio of unity versus NO_x mixing ratio. Symbols are the same as those described for Fig. 8.

Title Page
Abstract Introduction
Conclusions References
Tables Figures
◀| |▶
◀ ▶
Back Close
Full Screen / Esc
Printer-friendly Version
Interactive Discussion

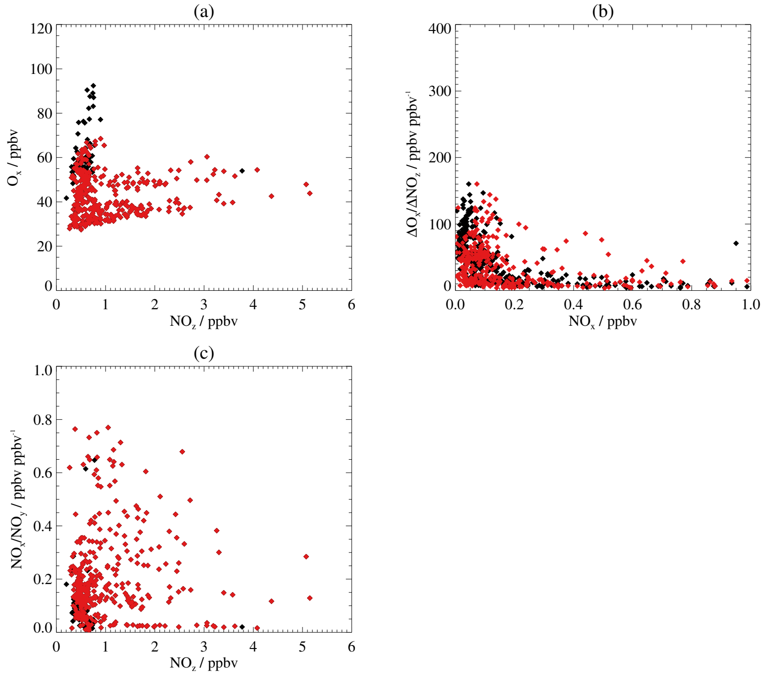

Fig. 12. Relationships between **(a)** O_x and NO_z, **(b)** $\Delta O_x/\Delta NO_z$ ratios and NO_x, and **(c)** the NO_x/NO_y ratio versus NO_z observed in boreal biomass burning plumes over Eastern Canada (110–50° W, 40–60° N) during the ARCTAS-B aircraft measurement campaign in the summer of 2008. Plume measurements are deteremined using an acetonitrile threshold of 150 pptv. Black and red diamonds show low aerosol and high aerosol plume measurements, respectively, determined from and black carbon mass concentration greater than 0.1 µg cm^{-1}.

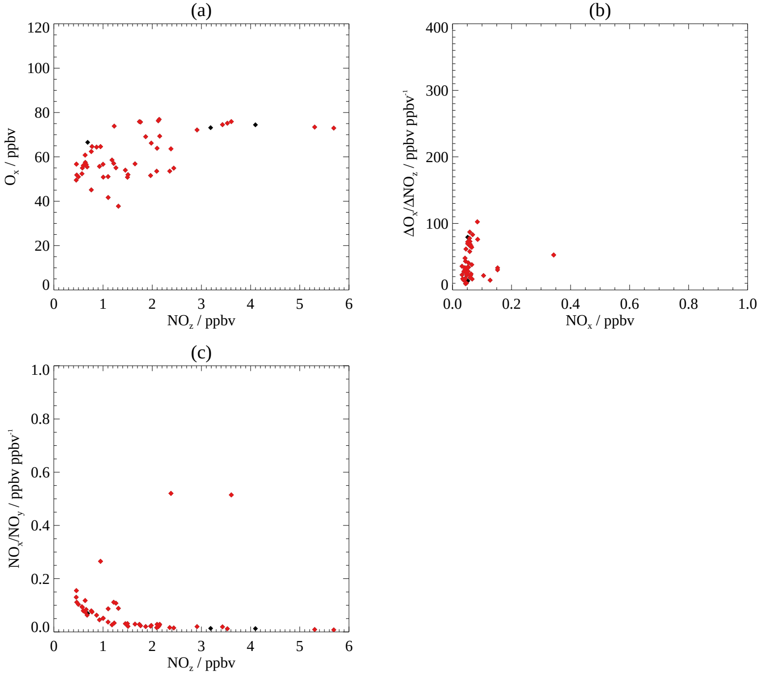

Fig. 13. Relationships between **(a)** O_x and NO_z, **(b)** $\Delta O_x/\Delta NO_z$ ratios and NO_x, and **(c)** the NO_x/NO_y ratio versus NO_z observed in boreal biomass burning plumes over Eastern Canada during the ABLE 3B aircraft measurement campaign in the summer of 1990. Plume measurements are determined for measurements of C_2Cl_4 less than 20 ppbv. Black and red diamonds show low aerosol and high aerosol plume measurements, respectively, determined from the concentration of fine (0.195–3.120 µm) and coarse (0.5–8.0 µm) particles.

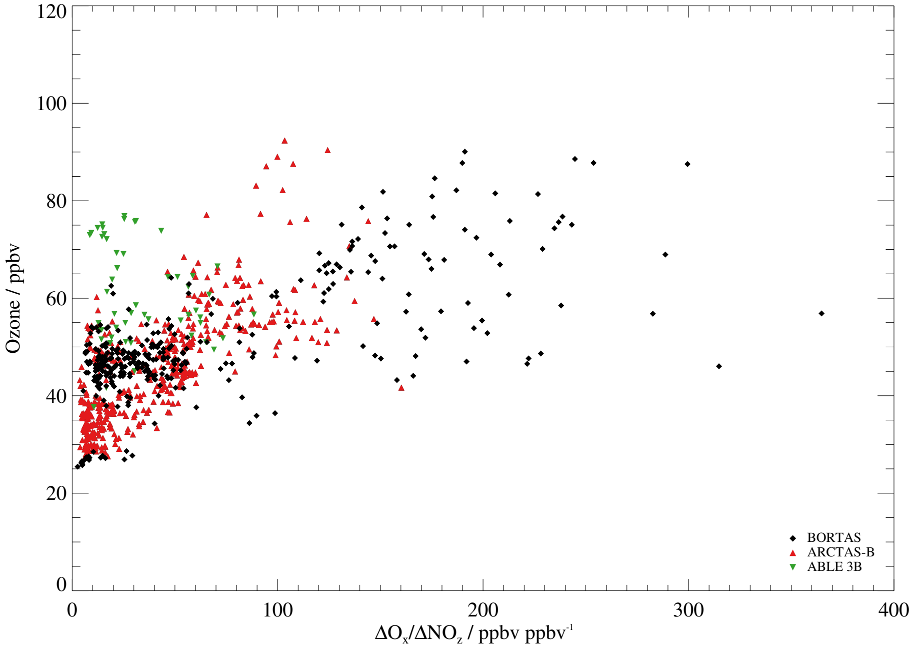

Fig. 14. Relationship between ozone mixing ratio and ozone production efficiency in boreal biomass burning plumes calculated from aircraft measurements made by the BORTAS (black diamonds), ARCTAS-B (red upward triangles), and ABLE 3B (green downward triangles) campaigns over Eastern Canada.